Gut microbial ecology of *Xenopus* tadpoles across life stages

Thibault Scalvenzi[1], Isabelle Clavereau[1], Mickaël Bourge[2] and Nicolas Pollet[1*]

1-Evolution, Génomes, Comportement & Ecologie, Université Paris-Saclay, CNRS, IRD, 91198 Gif-sur-Yvette, France

2-Institute for Integrative Biology of the Cell (I2BC), Université Paris-Saclay, CNRS, CEA, 91198 Gif-sur-Yvette, France

✷Corresponding author:
Nicolas Pollet
Laboratoire Evolution, Génomes, Comportement et Ecologie
CNRS
1 Avenue de la Terrasse
Batiment 13
F-91198 Gif-sur-Yvette
France
Tel: 33 01 69 82 37 10
Fax: 33 01 69 82 37 36

Abstract (350 words max)

Background: The microorganism world living in amphibians is still largely under-represented and under-studied in the literature. Among anuran amphibians, African clawed frogs of the *Xenopus* genus stand as well-characterized models with an in-depth knowledge of their developmental biological processes including their metamorphosis. In this study, we analyzed the succession of microbial communities and their activities across diverse body habitats of *Xenopus tropicalis* using different approaches including flow cytometry and 16s rDNA gene

metabarcoding. We also evaluated the metabolic capacity of the premetamorphic tadpole's gut microbiome using metagenomic and metatranscriptomic sequencing.

Results: We analyzed the bacterial components of the *Xenopus* gut microbiota, the adult gut biogeography, the succession of communities during ontogeny, the impact of the alimentation in shaping the tadpole's gut bacterial communities and the transmission of skin and fecal bacteria to the eggs. We also identified the most active gut bacteria and their metabolic contribution to tadpole physiology including carbohydrate breakdown, nitrogen recycling, essential amino-acids and vitamin biosynthesis.

Conclusions: We present a comprehensive new microbiome dataset of a laboratory amphibian model. Our data provide evidences that studies on the *Xenopus* tadpole model can shed light on the interactions between a vertebrate host and its microbiome. We interpret our findings in light of bile acids being key molecular components regulating the gut microbiome composition during amphibian development and metamorphosis. Further studies into the metabolic interactions between amphibian tadpoles and their microbiota during early development and metamorphosis should provide useful information on the evolution of host-microbiota interactions in vertebrates.

Keywords (3-10): Xenopus, Amphibian, Microbiome; Metamorphosis, Metagenome; Metatranscriptome

Background

Metazoans are vehicles for microbial communities, also named microbiota. The microbiota and its metazoan host have mutualistic interactions and are thought to adapt and evolve as an holobiont (Wilson and Sober, 1989; Gill *et al*., 2006; Zilber-Rosenberg and Rosenberg, 2008; Bordenstein and Theis, 2015). Several studies have highlighted the importance of the

52 microbiota in the function and development of several organs such as the alimentary canal, the
53 nervous system and the tegument (Sekirov *et al.*, 2010; Sommer and Bäckhed, 2013; Douglas,
54 2018). The dynamic interaction between a microbiota and its host is under intense scrutiny
55 especially for mammalian species and a handful of model organisms (Colston and Jackson,
56 2016; Douglas, 2019). However, very little is currently known on the biotic and abiotic
57 interactions between the microbiota of even well-known and classic vertebrate model
58 organisms such as amphibians (Colston and Jackson, 2016; Douglas, 2019; Rebollar and Harris,
59 2019).

60 The current paucity of knowledge on amphibian's microbiome is an historical thumb of
61 nose. Indeed in 1901, Olga Metchnikoff published a note on the influence of microbes on the
62 development of tadpoles (Metchnikoff, 1901). She concluded that microbes were vital to
63 tadpoles because they could not complete their development in sterile conditions, and her
64 results were confirmed by Moro (Moro, 1905). A few years later, these results were challenged
65 by Eugène and Elisabeth Wollmann, who finally observed that *Rana temporaria* tadpoles could
66 complete their metamorphosis in sterile conditions (Wollman, 1913). They also reported that
67 tadpoles could be fed solely with bacteria, pinpointing their nutritive roles (Wollman and
68 Wollman, 1915). Since that time, only few investigations have addressed the interactions
69 between bacteria and tadpoles during development.

70 Currently, the best-known amphibian model in biology is the African clawed frog. Several
71 features of its life cycle can facilitate investigations on the interactions between an animal host
72 and communities or individual microbial taxa. *Xenopus* have a long lifespan of more than ten
73 years and several tools are available to study their biology including genomic engineering
74 (Vouillot *et al.*, 2014). However, there are a few data on *Xenopus* microbiota. Mashoof et al.
75 used 16S rRNA metabarcoding to describe the bacterial diversity in the gut microbiota of adult

76 *Xenopus* and found that *Firmicutes*, *Bacteroidetes* and *Proteobacteria* were the dominant
77 bacterial phyla like in other vertebrates (Mashoof *et al*., 2013; Colombo *et al*., 2015).
78 Like many amphibians, *Xenopus* life history is characterized by an aquatic external
79 development. The embryo hatches after one or two days of embryonic development under the
80 protection of the chorion and of a double-layer jelly coat (Bles, E.J., 1906; Faber and
81 Nieuwkoop, 1994). The newly hatched embryo is in direct contact with its environment and
82 usually sticks to the remnants of its jelly coat thanks to secretions from its adhesive gland. The
83 mouth opens one day later, and after about two more days, the small tadpole starts feeding by
84 water filtration. Further growth and development continues during four weeks, a period called
85 premetamorphosis. During the next phase called prometamorphosis, limb growth is significant.
86 Finally, the end of morphogenesis is marked by tail resorption during the metamorphic climax
87 and the adult-shaped froglet is completely formed (Faber and Nieuwkoop, 1994; Brown and
88 Cai, 2007). Most organs, including the gut compartments, are found in both tadpoles and adults
89 but they experience a complete remodeling that enables the continuation of their physiological
90 functions in a different ecological niche (Hourdry *et al*., 1996; Heimeier *et al*., 2010).
91 Immunologically, post-embryonic development is hallmarked by significant changes
92 especially regarding mucosal immunity (Robert and Ohta, 2009; Pasquier, 2014; Colombo *et*
93 *al*., 2015). In particular, the climax of metamorphosis is hallmarked by high-levels of
94 glucocorticoids that cause a systemic immuno-depression (Rollins-Smith *et al*., 1997; Sachs
95 and Buchholz, 2019). Thus, amphibian metamorphosis is a post-embryonic developmental step
96 during which host-microbial interactions can play critical roles.
97 Amphibian tadpoles are almost invariably water-dwelling organisms, and most are
98 microphagous with microbial fermentation contributing up to 20 % of the energy uptake in
99 bullfrog (Clayton, 2005; Pryor and Bjorndal, 2005; Altig *et al*., 2007). After metamorphosis,
100 froglets are still microphagous but they start preying on larger animals as they grow, with a diet

101 composed predominantly of chitin-rich insects and other arthropods. The precise timing of
102 organ and behavioral modifications depends on ecological traits and is known in only a handful
103 of species, including *Xenopus*. As a *Pipidae*, *Xenopus* tadpoles, metamorphs, froglets and adult
104 frogs live predominantly in water (Bles, E.J., 1906).

105 Changes in gut bacterial communities during anuran metamorphosis was first studied using
106 culturing methods and more recently using 16S rDNA gene metabarcoding (Fedewa, 2006;
107 Kohl *et al*., 2013; Vences *et al*., 2016; Chai *et al*., 2018; Warne *et al*., 2019; Long *et al*., 2020;
108 Zhang *et al*., 2020). These very interesting studies reported changes in the composition of
109 microbial communities upon metamorphosis, with differences between species. A single study
110 expanded its analysis using metagenomic and metatranscriptomic (Zhang *et al*., 2020). Some
111 limitations of these studies are that they worked on natural populations of non-model organisms
112 without genomic resources. In addition, they typically sampled a single developmental stage
113 and they relied exclusively on DNA extracted from gut samples, yet we are unsure whether this
114 represents viable bacteria (Emerson *et al*., 2017).

115 Our goal in this work was to survey the phylogenetic and metabolic profiles of the gut
116 microbiota from *Xenopus* tadpoles during development and metamorphosis. We describe the
117 gut microbiome communities found at different life stages and their activities, the communities
118 found in different adult organs, including the skin, stomach, intestine and rectum and the effect
119 of the diet on tadpole's gut bacterial communities. We also investigated the transmission of
120 bacterial communities between parents and their eggs. Finally, we explored host-gut microbiota
121 metabolic interactions using functional annotations of the tadpole metagenome with the goal of
122 expanding our understanding of its functional potential.

123

124 # Results

125 ## Enumeration of bacterial cells in *Xenopus* tadpole's gut during development

126 We started to assess changes in tadpole's gut communities throughout development by
127 enumerating bacteria using flow cytometry (Figure 1). We selected six developmental stages
128 from young tadpoles that just started to feed up to adulthood, through grown-up tadpoles
129 undergoing metamorphosis (Figure 1A and Figure_S1). When we analyzed the distribution of
130 bacterial populations by relative cell size and DNA content, we found that cytometric profiles
131 differed according to life stages (Figure 1A). We observed distinct bacterial populations in
132 mature tadpoles compared to young ones (e.g. populations 50-3 and 56-4 absent or extremely
133 reduced in NF45 tadpoles, Figure 1A and Figure_S1). We also observed distinct cell
134 populations in froglet and adult guts (population Juv-4 and Adu-3 for example, Figure 1A and
135 Figure_S1). These first observations showed qualitative differences in the gut microbiomes
136 across life stages.

137 We quantified the total bacterial populations and determined an average of $1x10^6$ bacteria
138 per individual at the young tadpole stage, $2x10^8$ at the prometamorphic stage and $3x10^7$ in the
139 froglets (Figure 1B), indicating that the gut bacterial mass increased just after the beginning of
140 feeding and decreased simultaneously with the gut size reduction occurring during
141 metamorphosis (Schreiber *et al.*, 2005). We found that the bacterial load changed significantly
142 during development (ANOVA P-value = 0.041). The increase between pre-feeding and
143 prometamorphic tadpoles was significant (Tukey adjusted P-value = 0.046). We also observed
144 a tendency for a decrease between prometamorphic tadpoles and adults (Tukey adjusted P-value
145 = 0.073); and between prometamorphic tadpoles and froglets (Tukey adjusted P-value = 0.060).

146 We conclude from these cytometric data that there are qualitative and quantitative
147 differences in the gut microbiota across *Xenopus* life stages. The tadpole's gut is colonized by
148 a large population of bacteria at the beginning of feeding, and this bacterial population increases
149 during tadpole's development, then reduces upon metamorphosis before increasing again upon
150 froglet growth.

151 ## *Xenopus* gut microbial diversity during development and metamorphosis

152 Since our cytometry results pointed to the presence of an important bacterial population in
153 the tadpole's guts, we went on to quantify the taxonomic diversity of this microbiota during
154 development. We set out experiments in which we sampled whole tadpole's guts at different
155 life stages up to adulthood and quantified bacterial taxonomic diversity using 16S rRNA gene
156 profiling. We compared 16s rRNA gene profiles amplified from tadpoles at the premetamorphic
157 stages of development (tadpoles, NF54 to NF56, N=8), at the prometamorphic stages
158 (prometamorphs, NF58 to NF61, N=6), at metamorphic stages (metamorphs, NF 62, N=5), at
159 the end of metamorphosis (froglet, NF66, N=6) and from sexually mature adults (N=8). After
160 filtering low abundance and singleton sequence clusters, we obtained an abundance table for a
161 set of 666 OTUs. According to rarefaction and species accumulation curves, we obtained a
162 depth of sequencing sufficient to obtain a fair evaluation of the richness for the most abundant
163 bacterial species (Figure_S2).

164 We examined which bacteria constituted these most abundant gut communities (Figure 2
165 and Figure S3). We observed both global variations in bacterial phyla composition between
166 samples from different life stages (Figure 2A) and inter-individual variations between samples
167 from the same life stage (Figure 2C). In most cases, inter-individual variations were coherent
168 with the global changes observed with the previous or the next life stage, and for this reason
169 we pooled the observations from different samples belonging to the same life stage category
170 for further analysis.

171 At the premetamorphic stage of development, we observed that *Actinobacteria* dominated
172 the tadpole's gut microbiota (Figure 2A). At this stage, *Proteobacteria* (mostly
173 *Alphaproteobacteria*) and *Firmicutes* were also abundant while *Bacteroidetes* and
174 *Verrucomicrobia* contributions were quantitatively modest. The tadpole's gut microbiota
175 composition changed with *Proteobacteria* becoming the major phylum (mostly

176 *Deltaproteobacteria*) in prometamorphic tadpoles, followed by *Firmicutes*, *Actinobacteria*,
177 *Bacteroidetes*, *Synergistetes* and *Verrucomicrobia*. The proportion of *Proteobacteria* increased
178 in metamorphic tadpoles (mostly *Alphaproteobacteria*), *Firmicutes* abundance decreased and
179 *Bacteroidetes*, *Actinobacteria*, *Synergistetes* and *Verrucomicrobiae* were minor contributors.
180 Once metamorphosis was completed, the gut microbiome of the froglets changed and
181 *Firmicutes* became dominant, followed by *Proteobacteria* (mostly *Deltaproteobacteria*),
182 *Bacteroidetes*, *Actinobacteria*, *Synergistetes* and *Verrucomicrobia*. In comparison, the
183 composition of the adult gut microbiome was marked by more balanced abundances of
184 *Proteobacteria* (mostly *Deltaproteobacteria*) and *Firmicutes*, a remarkable abundance of
185 *Verrucomicrobia* (slightly higher than that of *Bacteroidetes)*, and a minor contribution of
186 *Synergistetes* and *Actinobacteria*. The abundance patterns for *Proteobacteria* were marked by
187 different contributions of *Alpha* and *Deltaproteobacteria*.

188 These patterns of abundances at the phylum level were attributable to a restricted number
189 of families (Figure 2B). At the family level, three genera from three families of *Bacteroidetes*
190 were predominant: *Bacteroides* (*Bacteroidaceae*) with a marked abundance increase at froglet
191 and adult stage, and *dgA-11* (*Rikenellaceae*) with an increase during tadpole growth and then
192 in adult stages, and *Parabacteroides* (*Porphyromonadaceae*) that increased only at the adult
193 stage. *Verrucomicrobiaceae* was the dominant family of *Verrucomicrobia* in adult guts, and it
194 was represented by a single genus, *Akkermansia*. Similarly, a single unknown genus of the
195 *Synergistaceae* family was found at low abundance in prometamorphic tadpoles and in adults.
196 *Synergistetes Microbacteriaceae* was the dominant family of *Actinobacteria* in pre and
197 prometamorphosis tadpole's guts, and it was represented by a single genus, *Leifsonia*. Seven
198 families of *Firmicutes* were predominant: *Lachnospiraceae* (several genera) and
199 *Peptostreptococcaceae* (one unknown genus) with a marked abundance increase at froglet and
200 adult stage; *Planococcaceae* (one unknown genus) that increased only at the adult stage;

201 *Clostridiaceae 1* (genus "*Clostridium sensu stricto 1*"), *Erysipelotrichaceae* (two genera
202 *Coprobacillus* and *Erysipelatoclostridium*) and *Ruminococcaceae* (genera
203 *Hydrogenoanaerobacterium*, *Anaerotruncus*, *Ruminococcaceae*) were found with fluctuating
204 abundances across the life stages, and finally *Family XIII* was found only at low abundance.
205 Eight families of *Proteobacteria* were predominant: *Aeromonadaceae* (genus *Aeromonas*),
206 *Neisseriaceae* (genus *Vogesella*) and a family of *Rhizobiales* (one unknown genus) dominated
207 the froglet gut microbiome; *Rhodospirillaceae* (one unknown genus) exhibited a tendency to
208 decrease across development and were minor in adults; *Desulfovibrionaceae* (genus
209 *Desulfovibrio*) were a minority at premetamorphosis and were abundant in the other stages,
210 *Pseudomonadaceae* (genus *Pseudomonas*) and *Bradyrhizobiaceae* (unknown genus) were
211 found in metamorph's guts, and *Rhodocyclaceae* (genus *Azovibrio*) in prometamorphic
212 tadpoles.

213 Altogether, we observed changes in the composition of the five most abundant bacterial
214 phyla making the gut microbiome as development proceeds, both during tadpole growth and
215 metamorphosis. The major shift during tadpole growth was a reduction of *Actinobacteria* and
216 an increase of *Proteobacteria*, and the transition to the adult lifestyle was marked by the
217 increase of *Synergistetes*, *Verrucomicrobia* and *Firmicutes*. This corresponds to a graded
218 increase of Gram-negative bacteria during tadpole growth and development culminating at
219 metamorphosis before reducing thereafter (Figure 2D).

220 We also analyzed changes of the estimations of OTU richness and phylogenetic diversity during
221 development (Figure S3, Supplementary_table_2). We identified two important and significant
222 changes: the first was an increase of bacterial species number and diversity that occurred during
223 tadpole growth between pre and prometamorphosis (p=0.000 using betta and the breakaway
224 estimation of richness); and the second was the opposite, namely a significant drop in species
225 richness and diversity that occurred at the climax of metamorphosis (Figure S3 and

226 Supplementary_table_2, (p=0.000 using betta and the breakaway estimation of richness). When
227 focusing on a tadpole-adult comparison, we found that the adult *Xenopus* gut microbiome
228 contained about twice more OTUs than the tadpole one, and its phylogenetic diversity was 1.8
229 times higher. These differences in microbiome diversity between the premetamorphic tadpole's
230 guts and the adult ones were significant using various alpha diversity metrics (Figure S3 and
231 Supplementary_table_2).

232 In parallel to these changes of communities across development, numerous OTUs were
233 shared between life stages. We found 111 OTUs (17%) present at all stages and representing
234 22% of the adult gut microbiome and 29 to 38% of the other life stage microbiomes
235 (Figure_S4). Another set of 128 OTUs was shared between four life stages, 122 OTUs were
236 shared between three, 151 between two and only 154 OTUs (23%) were found in only one of
237 the developmental stages (Figure_S4). The most prevalent OTUs were detected with a threshold
238 of very low relative abundances (< 5e-05 %, Figure_S4B). Nevertheless, we found a set of ten
239 OTUs that were both common and abundant including an *alpha proteobacterium*, three
240 *Desulfovibrio*, a *Microbacterioaceae*, a *Clostridium stricto sensu*, two
241 *Hydrogenoanaerobacteria*, a *Rhizobiales* and a *Lachnospiraceae* (Figure_S4E). The
242 abundances of the *Alphaproteobacteria*, one *Desulfovibrio*, the *Clostridium sensu stricto* and
243 the *Lachnospiraceae* were the most homogeneous (Figure_S4E).

244 We searched more specifically which OTUs were characterized by a significant change of
245 abundance across developmental stages using DESeq and identified a set of 22 OTUs
246 corresponding to five phyla and 13 known genera (Figure_S5). The five OTUs most abundant
247 in premetamorph tadpole's gut but not in adult's gut were a *Microbacteriaceae*
248 (*Actinobacteria*), a *Rummeliibacillus* and a *Clostridium sensu stricto* 13 (*Firmicutes*), a
249 *Bacteroides* (*Bacteroidetes*) and an *Alpha-proteobacteria* (*Proteobacteria*). The opposite
250 pattern, i.e. more abundant in adult's guts, was hallmarked by a *Lachnospiracae* (*Firmicutes*),

251 a *Synergistaceae* (*Synergistetes*), a *Ruminococcaceae UCG-014* (*Firmicutes*), a *Rhizobiales*
252 (*Proteobacteria*) and an *Anaerorhabdus furcosa* group (*Firmicutes*).

253 Significant differences in community composition (beta diversity) were evidenced by
254 microbial community phylogenetic structure and ordination analysis (Figure S3C,
255 Supplementary_table_2). The mean phylogenetic community structure and its dispersion
256 differed according to life stages (Figure_S6). The phylogenetic relatedness of communities
257 changed significantly during development, with negative and lower mean phylogenetic
258 diversity values found in metamorph and froglet samples indicating more phylogenetically
259 clustered microbial communities during metamorphosis. Overall, we conclude that the *Xenopus*
260 gut bacterial community succession during development and metamorphosis underwent
261 significant dynamic changes of composition and structure.

262 *Xenopus* microbiota across several gut compartments

263 To further compare the bacterial diversity along the gut of adult frogs, we dissected the gut
264 in three parts: stomach, intestine and rectum (N=3 for each tissue sample). In parallel, we
265 analyzed the bacterial composition of the feces and the skin of these animals using 16S rRNA
266 gene profiling (N=18 and N=20, respectively). Whereas *Bacteroidetes*, *Firmicutes* and
267 *Proteobacteria* were the most abundant bacteria in the intestines, the rectum, the feces and the
268 skin microbiota, we observed that the *Tenericutes* (mostly *Mollicutes*) were the most abundant
269 in the stomach (Figure 3A, Supplementary_table_2). Surprisingly we observed a large quantity
270 of *Acidobacteria* (28.8%) in only one feces sample. The stomach, intestine and rectum
271 microbiomes were well differentiated from each other in composition and in structure analysis
272 (PERMANOVA on bray-curtis dissimilarity $F=6.93$; $R2=0.43$; $p<0.001$, Figure 3B and
273 Supplementary_table_2). Feces and skin microbiomes were characterized by their largest
274 variability and were well separated along the x-axis in the ordination analysis.

275 Despite these differences, we identified 31 OTUs shared between the three gut sections: 16
276 were identified as *Bacteroidetes* (including 15 *Bacteroidia*), seven as *Firmicutes* (including six
277 *Clostridia*), six as Proteobacteria (including five *Desulfovibrio*), one *Parcubacteria* and one
278 *Synergistetes*. In conclusion, we showed that the bacterial diversity increased along the
279 anteroposterior axis of the adult *Xenopus* gut, from the stomach to the rectum, and the bacterial
280 community compositions and structures associated with those gut sections were also
281 significantly different (Supplementary_table_2).

282 **Activity of the *Xenopus* tadpole gut microbiome at the onset of feeding**

283 We then asked when bacterial communities started to be active during development and
284 what bacteria were found at the earliest stages of larval development. When *Xenopus* embryos
285 hatch, their mouth is not open, the archenteron is well formed and the post-anal gut is open.
286 Feeding behavior will only start once the mouth is formed and the gut organogenesis is more
287 advanced, a few days later (Chalmers and Slack, 1998). We took advantage of this life history
288 trait to perform a first investigation of the succession of active bacterial communities at early
289 stages of larval development just after hatching when the mouth is not open (NF 30), before
290 (NF41) and after feeding (NF48); and in growing premetamorphic tadpoles (NF50 and NF52).
291 We set out experiments in which we followed-up embryos and tadpoles from two egg clutches
292 up to the completion of metamorphosis. We targeted active bacteria by collecting RNA from
293 pools of whole embryos (N=2 using pools of 25 embryos) or tadpoles (N=2 using pools of 25
294 NF48, 20 NF50 or 5 NF52 tadpoles) starting at 24h after fertilization and performing 16S rRNA
295 gene sequencing.

296 We observed an increase of bacterial species number and diversity up to feeding stage,
297 followed by a transient reduction at stage NF50 (Figure_S7A). We found 103 OTUs present
298 across all stages, among which 11 were abundant OTUs (> 1%). At the earliest stage, we
299 observed that most bacterial activity was attributed to *Proteobacteria* (five OTUs:

300 *Rhodospirillaceae*, *Aeromonas*, *Rheinheimera*, *Pseudomonas*, *Desulfovibrio*) and
301 *Bacteroidetes* (two *Bacteroides* OTUs, one *Flectobacillus*, one *Rikenella*), that *Firmicutes*
302 (*Clostridium sensu stricto*) and *Synergistetes* (*Synergistaceae*) were already present while
303 *Fusobacteria* (*Fusobacteriales*) and *Verrucomicrobia* (*Akkermansia*) were minor contributors
304 (Figure_S7). We observed a different dynamic of bacterial community successions between the
305 two clutches. In one experiment, there was a gradual decrease of *Proteobacteria* between NF30
306 and NF50, and an increase thereafter at stage NF52. This was the opposite for *Bacteroidetes*.
307 In the other experiment, *Proteobacteriae* and *Synergistetes* abundances oscillated with a
308 decrease before and after feeding while the abundance of *Bacteroidetes* varied in an opposite
309 manner. This fluctuation was concomitant with a highest abundance of *Synergistetes* that
310 increased after feeding. In both clutches, *Firmicutes* proportion increased up to feeding stage
311 and decreased afterward. Altogether our results highlighted the presence of a rapidly developing
312 microbiota along the first stages of tadpole development, characterized by a shift of the
313 *Proteobacteria*/*Bacteroidetes* ratio.

314 We used the same strategy to monitor active bacterial communities in tadpoles at different
315 stages of metamorphosis using 16S rRNA sequencing on whole digestive tract RNA extracts
316 (N=2 using pools of five tadpole's guts). We analyzed the prevalence and the abundance of
317 bacteria as development proceeded. We found a common set of 33 OTUs present in at least 50
318 % of the samples with a relative abundance of 0.001% or more (Figure 4). All these OTUs were
319 also found at early stages before feeding, and in the gut of tadpoles up to the completion of
320 metamorphosis (Figure 4B). The five commonest OTUs were also the most abundant (> 0.01%
321 abundance), and included unknown or ill-defined species: a *Rikenella*, an *Alphaproteobacteria*,
322 a *Bacteroides*, a *Desulfovibrio* and a *Synergistaceae*. We found a few prevalent bacteria
323 detected with low abundances such as an *Alphaproteobacteria*, two *Ruminococcaceae*, a
324 *Rikenella* and an *Haliscomenobacter*.

325 In a complementary analysis, we used a Bayesian algorithm for source tracking to estimate
326 the proportion of OTUs populating the adult gut that originated from previous stages of
327 development (Figure_S7C) (Shenhav *et al*., 2019). In both experiments, the source of most
328 OTUs was identified as the feeding tadpole's gut (52 and 95%), a minority was identified as
329 stemming from the embryos (3 and 19%). Altogether, we identified that only few active bacteria
330 found in the embryos before the feeding stage will be later populating the adult gut, and that a
331 majority of tadpole's active bacteria will pass through metamorphosis and be also present in
332 the adult gut.

333 **Diet shapes *Xenopus* tadpole' gut active communities**

334 Since *Xenopus* tadpoles are suspension feeders, we hypothesized that tadpole's diets could
335 directly contribute to their active gut bacterial communities (Bles, E.J., 1906). We made an
336 experiment in which we fed tadpoles with a commonly used micro planktonic-based diet (food
337 1, N=9) or a custom meal (food 2, N=9), and monitored their gut microbiome composition
338 using 16S rRNA sequencing on RNAs. The micro planktonic food 1 contained a higher level
339 of fibers (6.4%) than food 2 (2.6%). The custom meal food 2 was sterile, devoid of chitin and
340 richer in available glucids (23.9%). The food regime did not change significantly tadpole
341 growth (Kruskal-Wallis chi-squared = 0.99, df = 1, p = 0.32) or development (Kruskal-Wallis
342 chi-squared = 0.34, df = 1, p = 0.56, Figure_S8). We found a total of 485 OTUs shared between
343 the tadpoles fed with one or another diet, and this was making up the majority of the OTUs
344 found in each condition: 485 out of 581, i.e. 83% for food 1 and 485 out of 531 i.e. 91% for
345 food 2. We did not observe significant changes of OTU richness ($\log_e$(W)=3.14, p=0.13) and
346 phylodiversity using Faith's index, ($\log_e$(W)=3.33, p=0.29). The differences of alpha-diversity
347 measured using the Shannon or the Simpson indices were significant ($\log_e$(W)=4.34, p=0.001
348 and $\log_e$(W)=4.30, p=0.004, respectively) pointing toward a higher specific richness in tadpoles
349 fed with food 1 (micro planktonic-based diet). This difference was confirmed by comparing

350 community structures: the mean standardized effect size of mean phylogenetic distances in
351 communities (SES MPD) was significantly different ($log_e(W)=0.69$, p=0.001), as did beta-
352 diversity spread (global PERMDISP F=13.42, df=1, N.perm=999, p=0.001). However, the
353 mean standardized effect size of mean nearest taxon distance (SES MNTD) was not
354 significantly different ($log_e(W)=3.93$, p=0.377). The gut bacterial community from tadpoles fed
355 on food 2 (custom meal) was globally more phylogenetically even (Figure_S8). The custom
356 meal was associated with more *Synergistetes* at the expense of *Firmicutes* and *Bacteroidetes*
357 (Figure 5). The taxonomic and phylogenetic composition of gut bacterial communities were
358 also significantly impacted by the diet (PERMANOVA on bray-curtis dissimilarity F=12.64,
359 R2=0.44, p=0.001 and on MNTD dissimilarity F=29.13, R2=0.64, p=0.001), as evidenced on
360 an ordination plot (Figure 5). The relative abundances of all five most abundant Phylum differed
361 according to the diet, the most notable being the *Synergistetes* that accounted for 0.05 to 0.76%
362 in the planktonic diet condition and for 0.80 to 17.72% in the sterile diet condition (Figure 5).
363 We found 82 OTUs whose abundance differed significantly according to diet (Figure_S8). For
364 example, *Chitinophagacae* were abundant in the tadpoles fed with the micro planktonic-based
365 diet, while a *Sphingobacteriales* was most abundant in tadpoles fed with the artificial diet.
366 Altogether, we observed that *Xenopus* tadpoles gut microbial communities could be shaped by
367 their diet without a noticeable impact on growth and development.

368 *Xenopus* microbiome transmission

369 The way bacterial communities are transmitted across individuals and generations is a recurrent
370 question in the study of animal microbiomes. We set out an experiment to evaluate the
371 inheritance of bacterial communities between *Xenopus* parents and their clutch of eggs. We
372 performed eight independent crosses and sampled the skin and the feces of both parents along
373 with their egg clutch (N=16, N=13 and N=8, respectively). When we looked at bacterial
374 diversity, we found that feces contained more *Verrucomicrobia* and *Firmicutes*, while both skin

375 and eggs contained more *Proteobacteria* (Figure 6). In one case, we observed a resemblance
376 between the communities of eggs and feces of one parent (Figure 6B). Globally, the bacterial
377 communities of the skin and of the eggs were significantly more similar to each other than those
378 from feces in terms of community structure and composition as evidenced using different
379 metrics (Figure 6BD, Supplementary_table_2). We also analyzed the proportion of the egg
380 bacteria derived from adult skin and feces using FEAST, a Bayesian algorithm for source
381 tracking (Shenhav *et al*., 2019). In five out of the eight crosses, more than 70% of the bacteria
382 found in the eggs did not come from feces or the skin of the parents. In the three other crosses,
383 we observed that male or female skin made up to 75% of the egg bacteria. In conclusion, we
384 found that the main driver of egg bacterial communities was the environment; the skin and the
385 feces of parents were only minor contributors.

386 Whole shotgun metagenomic and metatranscriptomic analysis of *X. tropicalis* 387 gut microbiota

388 In the final part of our analysis and since few studies have investigated the genomic
389 functions of the amphibian microbiome, we used a whole shotgun metagenomic and
390 metatranscriptomic approach to better characterize the *Xenopus* gut metagenome and its activity
391 in prometamorphic tadpoles (Figure 7). We obtained a dataset made of 23.6 and 19.8 million
392 paired reads using the metagenomic and metatranscriptomic approach, respectively after
393 filtering out reads mapping to the nuclear or the mitochondrial genome of *X. tropicalis*. We
394 used MATAM, phyloFlash, kraken2 plus bracken and kaiju to perform taxonomic assignation
395 of these reads against nucleotidic and proteic databases (Menzel *et al*., 2016; Pericard *et al*.,
396 2018; Wood *et al*., 2019; Gruber-Vodicka *et al*., 2020). As expected, bacterial reads were
397 predominant, but we identified also a few microeukaryotes, including various parasites (Figure
398 S9, Figure S10, Figure S11, Figure S12). We found low levels of reads assigned to Archaea
399 using kraken2/bracken and kaiju but these results turned out to be false positives upon closer

400 inspection. Indeed, more discriminant sequence comparison tools such as MATAM, phyloFlash
401 or megablast against SILVA or the NCBI non-redundant nucleotide databases evidenced that
402 these reads were of bacterial origin. We also found a few thousands bacteriophage viral
403 sequences using kraken2/bracken or kaiju but we did not investigate them in more details.

404 Metagenomic and metatranscriptomic sequencing gave similar taxonomic profiles for
405 bacteria according to the number of reads matching 16s rRNA gene sequences (Figure 7A).
406 Using phyloFlash on metagenomic reads, we assembled 16 near full-length SSU sequences
407 with phyloFlash-SPADES; 31 with phyloFlash-emirge and 33 using MATAM (Figure S9,
408 Figure S10). Using metatranscriptomic reads, we assembled 32 near full-length SSU sequences
409 with phyloFlash-spades; 1498 using phyloFlash-emirge and 440 using MATAM (Figure S11,
410 Figure S12). We observed four main dominant phyla: *Bacteroidetes* (mostly *Bacteroides*),
411 *Proteobacteria* (mostly *Desulfovibrio* and *Polynucleobacter*), *Firmicutes* (mostly
412 *Ruminococcus*) and *Actinobacteria* (mostly *Microbacterium*) (Figure 7A).

413 In conclusion, we confirmed that the *X. tropicalis* tadpole's gut microbiota harbors a large
414 amount and diversity of bacterial cells, mainly constituted of anaerobic bacteria and common
415 bacteria at the species level with other vertebrate's gut microbiota.

416 *Xenopus tropicalis* gut microbiota genes catalog

417 To characterize the *Xenopus* microbiome, we compiled a gene catalog from our
418 metagenome and metatranscriptome data sets. We assembled the metagenomic sequence reads
419 using different assemblers and compared the resultant assemblies with metaQUAST
420 (Mikheenko *et al.*, 2016). In addition, we mapped back all metagenomic and
421 metatranscriptomic reads and also our previously found OTU sequences (Supplementary table
422 3). We finally selected one assembly made using idba_ud, based on the rate of properly mapped
423 reads: 93.36% and 77.58% for DNA and RNA reads, respectively and on the number of OTUs
424 identified: 23 OTU sequences matching perfectly and 78 OUT sequences matching with 97%

425 identity to at least one contig. This assembly consisted of 72,183 contigs larger than 500 bp,
426 with a total assembly length of 161.8 Mbp. The contigs N50 size was 6,100 bp with the largest
427 contig being 640,454 bp long (Supplementary table 3). We then used DAStool to identify 22
428 bins covering 61.5 Mbp, including 14 bins with high completeness (> 90%) and low redundancy
429 (ie contamination, < 8%) (Figure 7B, Supplementary table 4). We found a single perfect
430 alignment of seven OTU sequences in seven different bins, and two bins containing two
431 unrelated OTUs each.

432 We predicted a total of 141,692 CDS using prokka on the tadpole metagenome assembly.
433 A subset of 87,012 CDS (61.4%) corresponded to hypothetical proteins. At least one
434 metatranscriptomic read could be mapped on 37,926 CDS (26.8%). For more than 95.0% of
435 these "expressed" CDS, the relative expression level was less than 100 reads per kilobase per
436 million (RPKM) while some were highly expressed with a relative expression higher than
437 10 000 RPKM.

438 In conclusion, we identified 141,692 CDS from the *X. tropicalis* tadpole gut metagenome.
439 Using metatranscriptomic sequencing, we revealed that about 27% of these protein encoding
440 genes are transcribed and therefore involved in a physiological activity.

441 Metabolic profile of the *Xenopus* gut microbiota

442 To better characterize the metabolic capacity of the *Xenopus* tadpole's gut metagenome, we
443 used a functional annotation strategy starting from the 141,692 predicted CDS. Out of these,
444 34,103 were annotated by prokka with a COG identifier and 32,801 by an EC enzyme number.
445 We used Minpath to identify 106 KEGG and 1,281 Metacyc metabolic pathways associated
446 with these known proteins (Ye and Doak, 2009 ; Figure 8A). Enzymatic activities linked to
447 degradation functions represented 48% of all predicted Metacyc pathways and those linked to
448 biosynthesis represented 45% (Figure 8A). Pathways involved in fermentation represented
449 0.8% and those involved in detoxification 0.5%. The detoxification potential provided by the

450 gut metagenome included chloroaromatic compounds and terpenoid degradation. A more
451 detailed view of the pathways predicted from the tadpole gut metagenome can be seen on the
452 Krona plots available in Figure_S13 and Figure_S14. Next, we compared the metabolic
453 pathways encoded by the *X. tropicalis* gut metagenome with those encoded by the *X. tropicalis*
454 genome (Figure_S15). To do so, we mapped the EC and KEGG identifiers associated to
455 metagenome-predicted CDS or to annotated *Xenopus* genes on the Interactive Pathway
456 Explorer (Darzi *et al.*, 2018). We queried the resulting pathway map using terms corresponding
457 to some of the numerous metabolites known to be derived from microbiome activity in
458 vertebrates (Figure 8B).

459 In herbivorous and omnivorous organisms, gut microbial communities are known to
460 degrade complex carbohydrate fibers and provide short chain fatty acids. We identified 6,823
461 genes encoding 205 different families of carbohydrate-active enzymes (89 glycoside hydrolase,
462 50 Glycosyltransferase, 16 Polysaccharide lyase, 16 Carbohydrate esterase and 32
463 Carbohydrate-Binding Modules as defined in www.cazy.org) and evidence that acetate,
464 propanoate and butyrate biosynthetic pathways were active in the *Xenopus* tadpole gut
465 metagenome (Figure_S16). We also looked for enzymes involved in nitrogen recycling and
466 found three CDS involved in N-fixation (*nifH);* 19 genes encoding urease that degrade urea
467 into ammonia and carbon dioxide (*ureABC)* and two genes encoding uricase homologs (*puuD)*.
468 Thus, tadpole's gut microbes are involved in nitrogen waste recycling to synthesize amino acids
469 and polypeptides that can act as nutrient sources. Indeed, we found that the known essential
470 amino-acids histidine, lysine and tryptophan could be produced by tadpole gut microbes (Figure
471 8B, Figure_S16). Another category of molecular exchange between the microbiota and its
472 vertebrate host involves the provision of vitamins (Magnúsdóttir *et al.*, 2015; Dearing and Kohl,
473 2017). We found evidences that various B-vitamins (folate, cobalamin, pantothenate,
474 riboflavin, biotin, thiamin and pyridoxin) and K-vitamin (menaquinone) could be synthesized

475 by the tadpole gut microbiota (Figure 8B, Figure_S14). Similarly, we identified expressed
476 bacterial genes encoding choloylglycine hydrolase involved in the biosynthesis of secondary
477 bile acids (Figure 8B). In conclusion, we identified a set of metabolic pathways from the tadpole
478 gut metagenome that are likely to influence tadpole's physiology through the action of different
479 metabolites.

480 **Discussion**

481 We report that a large community of bacteria develops in the tadpole alimentary canal as
482 soon as feeding starts and peaks before metamorphosis. While the gut microbiome biomass
483 diminishes significantly at metamorphosis, it remains important. This probably reflects the
484 feeding behavior of *Xenopus* at metamorphosis: Naitoh and colleagues reported that filter
485 feeding can be observed in metamorphs up to stage NF59-NF61, and adult-like feeding starts
486 at stage NF63 (Naitoh *et al*., 1989). Thus, there is only a short period of time, two to three days,
487 during which the *Xenopus* metamorph stops feeding. Also, the gut itself starts to shorten at the
488 metamorphic stage NF62 and will reduce four-fold to its adult-like length by stage NF66
489 (Schreiber *et al*., 2005; Heimeier *et al*., 2010). This means that adult feeding behavior occurs
490 before the completion of gut remodeling, and that tadpole and adult digestive physiology
491 overlap at the end of metamorphosis. In an animal-house setting, we deem it likely that *Xenopus*
492 froglets continue to eat the available plankton in the rearing aquarium as long as a new diet is
493 not artificially imposed to them, because they rely upon suction feeding as adults (Bles, E.J.,
494 1906). More generally, the change of eaten food composition is likely to be gradual depending
495 on the ecology of the amphibian species considered. For example, Fedewa reported insect
496 material in the guts of *Bufo terrestris* and *Pseudacris crucifer* at Gosner stage 45-46 (NF64-
497 NF65) i.e. in metamorph before the completion of metamorphosis, and the interval of fasting
498 was the beginning of metamorphosis (Gosner stages 42-44, NF60-NF63) (Fedewa, 2006).

499 Our metabarcoding data using DNA and RNA-based 16S rRNA gene sequencing further
500 demonstrated that the colonization of the tadpole by microorganisms occurred early during
501 *Xenopus* tadpole development. Moreover, our results proved that *Xenopus* gut bacterial
502 community composition changes during tadpole development and metamorphosis. At first, i.e.
503 before and right after feeding, the change in composition of the microbiota is characterized by
504 an increase of the *Bacteroidetes* / *Proteobacteria* ratio. The overall diversity of the microbiota
505 seems to be reduced just before feeding, possibly because of the development and the activity
506 of innate immune responses of the newly hatched larvae (Pasquier, 2014). After an increase of
507 the microbiota diversity once feeding started, there is another step of reduction that we interpret
508 as the result of an adaptation of the environmental bacterial population to the tadpole's gut
509 environment. In this period, when the tadpole starts feeding and grows rapidly (NF45 to NF56),
510 bacterial populations increase 1,000-fold but the microbiota composition remains quite the
511 same. During metamorphosis, we observed an important diminution of the bacterial abundance
512 and a change of diversity. Indeed metamorphosis is associated with several modifications of
513 the gut organs and we expected that gut reduction and neuroendocrine changes would impact
514 the gut microbiota, as shown previously for other species (Fedewa, 2006; Kohl *et al.*, 2013;
515 Vences *et al.*, 2016; Chai *et al.*, 2018; Warne *et al.*, 2019; Long *et al.*, 2020; Zhang *et al.*, 2020).
516 The bacterial diversity observed in the *X. tropicalis* gut was consistent with the results of
517 Mashoof et al. on the diversity observed in *X. laevis* gut (Mashoof *et al.*, 2013). Indeed, the
518 same three phyla dominating the gut microbiota were observed in both analyses. The
519 dominance of *Firmicutes*, *Bacteroidetes* and *Proteobacteria* is also a characteristic of the
520 vertebrate gut in general (Colston and Jackson, 2016; Youngblut *et al.*, 2019). Moreover the
521 *Xenopus* gut microbiota diversity increased following the anteroposterior axis of the gut, as
522 observed in human gut microbiota (Sekirov *et al.*, 2010). We did not detect Archaea using our
523 metabarcoding methodology, neither did we identify Archaea in our metagenomic and

524 metatranscriptomic data. While we expected to miss Archaea in metabarcoding sequences
525 because we relied on mainly bacteria-targeting primers, the lack of Archaea sequences in the
526 shotgun sequences was more surprising. This constitutes a limitation of our survey and an
527 interesting subject for further investigation in light of the account of methanogenesis in adult
528 *Xenopus* (Saengkerdsub and Ricke, 2014).

529 We found that the abundance of several *Bacteroides*, *Bilophila* and *Lachnospiraceae*
530 bacteria increase during tadpole development and metamorphosis. These bacteria are well-
531 known to be abundant in the gastro-intestinal tracts of numerous vertebrates, including humans,
532 and characterized by their resistance to high concentrations of bile salts or their bile acid
533 hydrolase activities (Song *et al*., 2019). In addition, we identified seven CDS encoding an
534 enzyme involved in secondary bile acid biosynthesis. We therefore propose an interpretation of
535 our findings in light of bile acids being key molecular components regulating the gut
536 microbiome composition during amphibian development and metamorphosis. Bile acids are
537 small molecules produced mainly in the liver from cholesterol and further metabolized in the
538 gastro-intestinal tract. They are known to act as molecular messengers between the host and
539 their gut microbiota: on the host side, they play a role in numerous metabolic pathways via their
540 cellular receptors and on the microbiome side they can modulate bacterial growth directly and
541 indirectly (Ridlon *et al*., 2014; Wahlström *et al*., 2016). Bile acids can act directly on the gut
542 microbiome because they have intrinsic antimicrobial activity and indirectly because their host
543 cellular receptors regulate antimicrobial peptides gene expression. In turn, some bacteria
544 encode bile hydrolases that enable the production of secondary bile acids (Joyce *et al*., 2014;
545 Song *et al*., 2019). Therefore, we can consider bile acid composition as a trait of strong
546 evolutionary significance since it links nutrition, gut, liver and gill physiology, host genome
547 evolution and the gut microbiome composition (Reschly *et al*., 2008; Hofmann *et al*., 2010;
548 Ridlon *et al*., 2014). In amphibians, bile acids are present in tadpoles but they increase in

549 quantity and complexity after metamorphosis (Anderson *et al*., 1979; Cole and Little, 1983;
550 Reschly *et al*., 2008). It is known that bile acids composition changes and complexity increases
551 due to changes in host gene expression. We hypothesize that ontogenetic and endocrine
552 regulation of amphibian host genes such as the bile acid nuclear receptor (Farnesoid X receptor,
553 FXR; NR1H4), or its surface G-protein coupled receptor (TGR5) could be initial regulators of
554 gut microbiome composition. FXR, an intra-cellular bile acid-sensing transcription factor of the
555 nuclear factor superfamily, regulates bile acid and lipid homeostasis, and other genes such as
556 FOR in *Xenopus* may play similar roles using different ligands (Seo *et al*., 2002; Reschly *et al*.,
557 2008; Frisch and Alstrup, 2018). It is noteworthy that in mice TGR5 has been shown to link
558 bile acid and thyroid hormone signaling by promoting intracellular thyroid hormone activity
559 via the induction of deiodinase 2 in brown adipose tissue (Watanabe *et al*., 2006). In future
560 studies, manipulation of gene activities, of bile acid composition and concentration and of the
561 microbiome could be used to unravel the diversity and the evolution of these regulations in
562 amphibians and other vertebrates.

563 We provide evidence that the diet of *Xenopus* tadpoles affected the diversity of their gut
564 microbiome and thus that the mucosal immunity of tadpoles can interact with a variety of
565 bacterial communities (Figure 5). Tadpoles fed a micro planctonic-based diet had a gut
566 microbiome with a higher specific richness compared with tadpoles fed a sterile flour-diet. The
567 latter diet was associated with a lack of *Chitinophagacae* involved in chitin degradation. These
568 results contribute to the growing body of evidence that diet as an environmental factor can
569 affect the composition of the gut microbiota.

570 Maternal transmission of microbes in animals is a well-known phenomenon but its
571 documentation in amphibians is restricted to only few examples (Funkhouser and Bordenstein,
572 2013; Walke *et al*., 2014; Warne *et al*., 2019). In amphibians like in other animals, the
573 transmission of microbial communities can be horizontal, vertical or environmental. The

574 vertical transmission mode may depend critically on the reproductive behaviour of the animals.
575 In *Xenopus,* the natural mating behaviour of the couple in amplexus involves looping dances
576 from the bottom to the surface. Eggs are mostly laid by the female when she is near the surface,
577 and immediately fertilized by the male. These movements may lead eggs to stick to the skin of
578 either parent, and since the skin of amphibians harbors a rich microbiota, it can constitute a
579 vector of vertical transmission from either parent. In addition, the eggs are laid through the
580 female cloaca, and the sperm is also emitted by the male cloaca. Since the cloaca is a common
581 anatomical structure shared by the reproductive, excretory and digestive systems, the microbial
582 communities of these three systems may be transmitted to the eggs. Here we sampled the skin
583 and feces of both parents to quantify the transmission of bacteria to the eggs. Quantitatively
584 and using the Bayesian algorithm of source tracker, we found that the bacteria found on the
585 eggs were mostly coming from the environment, and the second source was the skin of either
586 parent. It was notable that a *Chitinimonas* species, a bacterium known to synthesize the
587 antifungal Violacein, was one of the OTU transmitted from both parents in all crosses. This is
588 relevant in the context of *Saprolegnia* egg infections and chytridiomycosis. Recently, Warne
589 and collaborators reported that changes of the woodfrog egg microbiota influenced the bacterial
590 communities at later larval stages (Warne *et al*., 2017, 2019).

591 *Bacteroidetes*, *Firmicutes* and *Proteobacteria* were slightly more represented in the
592 metatranscriptome than in metagenome highlighting that those bacteria were present and active
593 in the tadpole gut. *Actinobacteria* were less abundant in metatranscriptome than metagenome,
594 showing a reduced activity. On the contrary, we found that *Verrucomicrobia* were very active.

595 Our data highlight the important capacity of the microbiota to complement the metabolic
596 pathways of the *Xenopus* genome. We found that the gut microbiota of tadpoles synthesizes
597 short chain fatty acids, essential amino acids and vitamins and recycle nitrogen waste products.

598 The need to perform investigations on animals from natural populations has rightly been
599 underscored, for example by an interesting review of Sarah Hird (Hird, 2017). Yet we face
600 several methodological difficulties when it comes to sample natural populations. In some
601 studies, animals have been captured in the wild and raised thereafter in a laboratory setting. The
602 current global threats on amphibians makes such studies difficult to realize and restricts
603 severely the breadth of species that can be studied. In addition, the capture of vertebrate animals
604 induces a variable amount of stress, leading to different responses including an
605 immunosuppression (Rollins-Smith *et al*., 1997; Narayan, 2013). While the effect of captivity
606 on amphibian microbiomes has been documented, there is a ample room for possible
607 explanations (Becker *et al*., 2014; Loudon *et al*., 2014; Bataille *et al*., 2016). Also, parasitism
608 is common in natural populations, and it can represent a hidden variable of considerable
609 importance in microbiome studies. For example, the mutualism between the nematode
610 *Gyrinicola batrachiensis* and *Rana catesbeiana* leads to a quicker tadpole development and has
611 been linked to the hindgut fermentation capacity (Pryor and Bjorndal, 2005). Studies on
612 laboratory animals for which rearing conditions are more uniform, with the potential for a better
613 control of parameters and for reproducing experiments in different laboratories are definitively
614 needed to make the link with investigations on natural populations. In this regard, *Xenopus*
615 represents an interesting model since it is a widespread anuran with more than 20 species
616 described in sub-Saharan Africa and classified of least-concern according to IUCN, and there
617 is a vast body of biological knowledge relating to its development, its physiology and its
618 genetic. We hope that our study will constitute a background knowledge enabling future work
619 in the study of amphibian-microbial symbioses.

620 There were several important limitations to this study. First, marker gene and metagenomic
621 studies are replete of confounding aspects and more studies will be needed to reproduce our
622 observations using alternative technologies and more samples to explore inter-individual

623 variability (Pollock *et al*., 2018; Bharti and Grimm, 2019; McLaren *et al*., 2019). This is
624 especially needed regarding the construction of a metagenome gene catalog. Second, we
625 analyzed the microbiome of *Xenopus* tadpoles in a laboratory setting and this is likely to differ
626 from animals sampled *in natura*. Third, we did not survey Archaea nor microeucaryotes that
627 are important players of the gut microbiome in other vertebrates and this will need dedicated
628 efforts.
629

630 # Conclusions

631 In summary, we described the bacterial components of the *Xenopus* gut microbiota, the
632 adult gut biogeography, the succession of communities during ontogeny, the impact of the
633 alimentation in shaping the tadpole's gut bacterial communities, the transmission of skin and
634 fecal bacteria to the eggs. We also identified the most active gut bacteria and their metabolic
635 contribution to the tadpole physiology. Keeping in mind the advantages of the *Xenopus* model,
636 our data provided evidences that *X. tropicalis* raised in animal facilities is highly suitable for
637 host-microbiota studies. Our study contributes to the growing body of research on the study of
638 bacterial symbiosis in amphibians and on the evolutionary associations between amphibians
639 and their microbiota. Further studies on the dynamics of the *X. tropicalis* gut microbiota during
640 early development and metamorphosis should provide useful information on the evolution of
641 host-microbiota interactions in vertebrates.
642

643 # Methods

644 ## Animals and animal husbandry

645 We used *Xenopus tropicalis* frogs from the TGA and Sierra Leone strains and we let them
646 reproduce using induced natural mating as described in the supplementary

647 Extended_materials_and_methods. Parents were transferred back to their housing tank while
648 the embryos were let in the mating tanks. Tadpoles were reared in static water throughout
649 embryogenesis and metamorphosis. Tadpoles and adults were euthanized with tricaine methane
650 sulfonate pH 7.5 at 5 $g.L^{-1}$. We used the Nieuwkoop and Faber table of development to identify
651 tadpole's developmental stages (Faber and Nieuwkoop, 1994).

652 **Tissue sampling**

653 We dissected euthanized tadpoles or adults in sterile amphibian phosphate buffered saline
654 (aPBS) to collect the gastro-intestinal from the stomach to the rectum. For the sake of
655 simplicity, we used the term "gut" to refer to the whole gastro-intestinal tract of tadpoles or
656 adults throughout the manuscript. Whole embryos and early tadpoles were abundantly rinsed
657 using aPBS before further processing. The skin of adult frogs was sampled after having
658 abundantly rinsed the animals using aPBS. Sampling was performed by swabbing the dorsal
659 and ventral skin areas using a sterile cotton swab. Feces were collected using a sterile Pasteur
660 pipette from frogs that were individually housed in aPBS after reproduction. Samples of two-
661 hundred eggs including their outer and inner jelly coat were collected using a sterile Pasteur
662 pipette from the reproduction aquarium, and washed three times in sterile aPBS. All tissue
663 samples used for DNA extraction and metabarcoding were then immersed in at least ten
664 volumes of ethanol and stored at -20°C until DNA extraction. All tissue samples used for RNA
665 extraction and metabarcoding were kept on ice and then processed for tissue lysis as explained
666 in the Supplementary Extended_materials_and_methods.

667 **Bacterial purification from intestinal tracts**

668 We homogenized each freshly dissected intestinal tract in 500 µL of ice-cold PBS using a
669 Potter-Elvehjem homogenizer. We then concentrated the bacteria extract by successive
670 filtrations on 40, 20 and 5 µm filters (nylon 40 µm cell strainer from BIOLOGIX; 20 µm net
671 ring from Pharmacia Fine chemicals; Whatman® Puradisc 13 syringe filters 5 µm from

672 SIGMA-ALDRICH®). Next, we harvested the cells by centrifugation at 13 000g for 15 min at
673 room temperature. These pellets were then used for nucleic acid extraction (details in
674 Supplementary Extended_materials_and_methods) or fixation and microscopy (for quality
675 control) or flow cytometry analysis.

676 **Flow cytometry analysis**

677 We prepared triplicate samples from tadpoles at stages NF45-48, NF51-54, NF56, NF60-
678 61, 15 days froglets and adults. Each sample was made from five tadpole's guts per replicate
679 for the NF45-48 and NF51-54 stages, single individuals were used for later developmental
680 stages. We fed the tadpoles two days before the first time point (stage NF45-48), and ten days
681 before sampling the froglets. We prepared the filtered bacterial cell samples as described
682 previously and we fixed the resuspended bacterial pellet in 1.0% paraformaldehyde at 4°C
683 during 2 h. We analyzed samples prepared by mixing bacterial samples with fluorescent beads
684 (Flow-Count™ fluorospheres, 10 μm diameter, 1010 beads/μl) to obtain a final concentration
685 of 20 beads/μl. Bacterial samples were stained using propidium iodide (PI) with a MoFlo®
686 Astrio™ cytometer (BECKMAN COULTER). Excitation was made at 488 nm and 561 nm for
687 scattering (Forward Scatter, FSC; Side Scatter, SSC) and PI respectively. Emission of PI was
688 collected through a 614/20-nm band pass filter. Each measure was done in triplicate to compute
689 a mean value and the standard deviation for each biological replicate sample. Plots were
690 normalized on 200,000 gated events for the analysis of cell populations.

691 **Metagenome and metatranscriptome sequencing**

692 We prepared genomic DNA (gDNA) and RNA from freshly prepared 5 µm filtered gut
693 samples prepared as previously described and obtained from five *X. tropicalis* tadpoles at stage
694 NF56 raised in the same aquarium. We obtained 10-15 μg of total RNA and ~1 μg of DNA per
695 filtered tadpole gut. Metagenomic and metatranscriptomic library construction and sequencing
696 were performed by the Beijing Genomics Institute (BGI) using an Illumina® HighSeq™ 2500.

697 The insert sizes of the metagenomic and metatranscriptomic libraries were 170 bp and 180 bp,
698 respectively. We obtained 47,279,786 and 40 000 000 high quality 100bp paired end sequences
699 for metagenomic (ERS716504) and metatranscriptomic (ERS716505), respectively.

700 16S rRNA and 16S rDNA library construction and sequencing

701 We prepared genomic DNA (gDNA) from dissected tissue samples that were fixed in
702 ethanol and stored at -20°C before processing. RNA was prepared from fresh tissue. gDNA or
703 RNA were used as template for 16S Ribosomal RNA (16S rRNA) or DNA (16S rDNA)
704 amplification. A detailed list of samples used for the 16S rDNA and rRNA library construction
705 is given in Supplementary_table_1. A first set of three replicate PCR reactions was performed
706 to amplify the V3-V4 variable region of the 16S rDNA and rRNA; the PCR condition details
707 and oligonucleotide sequences are given in Supplementary Extended_materials_and_methods.
708 The PCR products were sent to the GeT sequencing facility (France Génomique, INRAE,
709 Toulouse) for library preparation and sequencing. PCR products were purified and quantified
710 by spectrophotometry and a second PCR was performed to integrate a barcode index. The
711 barcoded PCR products were pooled and their quality was checked using capillarity
712 electrophoresis and quantitative PCR. Finally, the PCR products were sequenced using a Miseq
713 (supplied by Illumina®). We obtained a total of 3,647,548 clean read counts from 132 samples,
714 with a minimum of 23,872, a maximum of 179,732 and a median of 43,174 reads. The metadata
715 and number of sequences obtained by sample is given in Supplementary_table_1.

716 16S rRNA and 16s rDNA sequence analysis

717 We used the FROG pipeline for OTUs identification and taxonomic affiliation (Escudié *et*
718 *al*., 2018). Overlapping reads were assembled and sequences were dereplicated before
719 clustering using the SWARM algorithm. Chimeric sequences were then removed and OTUs
720 were filtered on abundance for at least 0.005%. Taxonomic affiliation of the OTUs was
721 performed based on the 16S SILVA database (V.123) using blast and RDP classifier.

722 We used script implemented in R to perform different microbiome community analysis
723 (provided on GitHub at https://npollet.github.io/metatetard/) (R Core Team, 2019). Source-
724 sink analysis was performed using Feast (Shenhav *et al*., 2019).

725 Taxonomic assignment for metagenome and metatranscriptome sequences

726 We used MATAM and phyloFlash to extract and assemble full-length or near full-length
727 16S and 18S rRNA gene sequences from the same set of filtered reads as the one used for the
728 assembly (Pericard *et al*., 2018; Gruber-Vodicka *et al*., 2020). The assembled read and the
729 details of the command lines are provided on GitHub at
730 https://npollet.github.io/metatetard/Metagenome.html).

731 Metagenome assembly and gene prediction

732 We filtered and trimmed reads according to their quality and excluded those derived from
733 *Xenopus* genome using metaWRAP. We selected one assembly of these reads obtained with
734 IDBA-UD using k-mers from 72 to 124 (Peng *et al*., 2012; Uritskiy *et al*., 2018). More details
735 are given in the Supplementary Extended_materials_and_methods. We performed binning on
736 contigs longer than 1000 bp using maxbin, concoct, metabat and DAStool (Alneberg *et al*.,
737 2014; Wu *et al*., 2016; Sieber *et al*., 2018; Kang *et al*., 2019). We visualized binning results
738 using vizbin (Laczny *et al*., 2015). We mapped OTUs, metagenome and metatranscriptome
739 reads to the assembly using BBTools to derive coverage and tpm values at the scaffold and
740 gene levels (BBMap).

741 We predicted CDS on the assembled metagenome scaffolds using Prokka (Seemann, 2014).
742 We used Minpath for metabolic pathway prediction following the strategy and the tools
743 provided in the IMP pipeline scripts as described in https://metagenomics-
744 workshop.readthedocs.io (Ye and Doak, 2009; Narayanasamy *et al*., 2016). We mapped KEGG
745 and EC identifiers on the Interactive Pathway Explorer V3 (iPATH3) to obtain a map of the
746 tadpole's gut microbiota metabolic pathway (Darzi *et al*., 2018).

List of abbreviations

NF: Nieuwkoop and Faber developmental stage

Declarations

Ethics approval and consent to participate: We used standard rearing conditions for *Xenopus* tadpoles and adults and all animal experiments were conducted in accordance with the regulation on Animal Experimentation (registration number 91–401 provided by Direction Départementale des Services Vétérinaires de l'Essonne).

Consent to publication:

Not applicable

Availability of data and material: The sequence datasets generated and/or analyzed during the current study are available in the EMBL Nucleotide Sequence Database (ENA), metagenomic (ERS716504) and metatranscriptomic (ERS716505) https://www.ebi.ac.uk/ena/data/view/PRJEB9311. 16S rRNA gene sequence data are available at https://www.ebi.ac.uk/ena/data/view/PRJEB38248. OTU sequences are available at http://www.ebi.ac.uk/ena/data/view/LR992138-LR992913. R scripts for data analysis are provided on GitHub at https://npollet.github.io/metatetard/.

Other data type supporting the findings are available within the article and its supplementary files.

Competing interests: The authors declare that they have no competing interests.

Funding:

We used the Data Intensive Academic Grid conducted on the National Science Foundation funded MRI-R2 project #DBI-0959894" to perform some of the bioinformatic analyses. The cytometry facilities of Imagerie-Gif (http://www.i2bc.paris-saclay.fr/spip.php?article279) is

member of the Infrastructures en Biologie Santé et Agronomie (IBiSA), and is supported by the French National Research Agency under Investments for the Future programs "France-BioImaging", and the Labex "Saclay Plant Science" (ANR-10-INSB-04-01 and ANR-11-IDEX-0003-02, respectively).

Author's contributions: All authors read and approved the final manuscript. TS and IC performed experimental work under the guidance of NP. MB designed and supervised TC for cytometry, and analyzed cytometry results. TC performed whole genome shotgun sequence analysis. NP performed 16S rRNA gene sequence analysis. TS and NP wrote the manuscript.

Acknowledgements

We are grateful to the Genotoul bioinformatics platform Toulouse Midi-Pyrenees (Bioinfo Genotoul) for providing computing and storage resources at the start of this project. The present work has benefitted from the facilities and expertise of the cytometry facilities of Imagerie-Gif, (http://www.i2bc.paris-saclay.fr/spip.php?article279). We thank Catherine Zanchetta and the team of the GeT facility for 16S metabarcoding sequencing. We thank Odile Bronchain, Albert Chesneau and Muriel Perron for providing access and use of their *Xenopus* animal facility in Orsay. We thank Yves Carton for pointing us the work of Olga Metchnikoff. We thank Franck Bourrat and Jean-Michel Rossignol for critically reading our manuscript. We are thankful to the reviewers for taking the time to review this manuscript. Their comments and suggests have greatly improved the manuscript.

Conflict of Interest

None

References (100 max)

Alneberg, J., Bjarnason, B.S., de Bruijn, I., Schirmer, M., Quick, J., Ijaz, U.Z., et al. (2014) Binning metagenomic contigs by coverage and composition. *Nat Methods* **11**: 1144–1146.

Altig, R., Whiles, M.R., and Taylor, C.L. (2007) What do tadpoles really eat? Assessing the trophic status of an understudied and imperiled group of consumers in freshwater habitats. *Freshw Biol* **52**: 386–395.

Anderson, I.G., Briggs, T., Haslewood, G.A., Oldham, R.S., Schären, H., and Tökés, L. (1979) Comparison of the bile salts of frogs with those of their tadpoles. Bile-salt changes during the metamorphosis of Rana Catesbeiana Shaw. *Biochem J* **183**: 507–511.

Bataille, A., Lee-Cruz, L., Tripathi, B., Kim, H., and Waldman, B. (2016) Microbiome Variation Across Amphibian Skin Regions: Implications for Chytridiomycosis Mitigation Efforts. *Microb Ecol* **71**: 221–232.

BBMap *SourceForge*.

Becker, M.H., Richards-Zawacki, C.L., Gratwicke, B., and Belden, L.K. (2014) The effect of captivity on the cutaneous bacterial community of the critically endangered Panamanian golden frog (Atelopus zeteki). *Biol Conserv* **176**: 199–206.

Bharti, R. and Grimm, D.G. (2019) Current challenges and best-practice protocols for microbiome analysis. *Brief Bioinform*.

Bles, E.J. (1906) The life history of Xenopus laevis, Daud. *Trans R Soc Edin* **41**: 789–821.

Bordenstein, S.R. and Theis, K.R. (2015) Host Biology in Light of the Microbiome: Ten Principles of Holobionts and Hologenomes. *PLoS Biol* **13**: e1002226.

Brown, D.D. and Cai, L. (2007) Amphibian metamorphosis. *Dev Biol* **306**: 20–33.

Chai, L., Dong, Z., Chen, A., and Wang, H. (2018) Changes in intestinal microbiota of Bufo gargarizans and its association with body weight during metamorphosis. *Arch Microbiol* **200**: 1087–1099.

Chalmers, A.D. and Slack, J.M. (1998) Development of the gut in Xenopus laevis. *Dev Dyn Off Publ Am Assoc Anat* **212**: 509–521.

Clayton, L.A. (2005) Amphibian gastroenterology. *Veterinary Clin North Am Exot Anim Pract* **8**: 227–245.

Cole, K.D. and Little, G.H. (1983) Bile pigments and bilirubin UDP-glucuronyl transferase during the metamorphosis of Rana catesbeiana tadpoles. *Comp Biochem Physiol B* **76**: 503–506.

Colombo, B.M., Scalvenzi, T., Benlamara, S., and Pollet, N. (2015) Microbiota and mucosal immunity in amphibians. *Front Immunol* **6**: 111.

Colston, T.J. and Jackson, C.R. (2016) Microbiome evolution along divergent branches of the vertebrate tree of life: what is known and unknown. *Mol Ecol* **25**: 3776–3800.

Darzi, Y., Letunic, I., Bork, P., and Yamada, T. (2018) iPath3.0: interactive pathways explorer v3. *Nucleic Acids Res* **46**: W510–W513.

Dearing, M.D. and Kohl, K.D. (2017) Beyond Fermentation: Other Important Services Provided to Endothermic Herbivores by their Gut Microbiota. *Integr Comp Biol* **57**: 723–731.

Douglas, A.E. (2018) Fundamentals of Microbiome Science: How Microbes Shape Animal Biology, Princeton: Princeton University Press.

Douglas, A.E. (2019) Simple animal models for microbiome research. *Nat Rev Microbiol* **17**: 764–775.

Emerson, J.B., Adams, R.I., Román, C.M.B., Brooks, B., Coil, D.A., Dahlhausen, K., et al.

842 (2017) Schrödinger's microbes: Tools for distinguishing the living from the dead in microbial
843 ecosystems. *Microbiome* **5**: 86.
844 Escudié, F., Auer, L., Bernard, M., Mariadassou, M., Cauquil, L., Vidal, K., et al. (2018)
845 FROGS: Find, Rapidly, OTUs with Galaxy Solution. *Bioinformatics* **34**: 1287–1294.
846 Faber, J. and Nieuwkoop, P.D. (1994) Normal Table of Xenopus Laevis, 1 edition. New
847 York: Garland Science.
848 Fedewa, L.A. (2006) Fluctuating Gram-Negative Microflora in Developing Anurans. *J*
849 *Herpetol* **40**: 131–135.
850 Frisch, K. and Alstrup, A.K.O. (2018) On the Evolution of Bile Salts and the Farnesoid X
851 Receptor in Vertebrates. *Physiol Biochem Zool PBZ* **91**: 797–813.
852 Funkhouser, L.J. and Bordenstein, S.R. (2013) Mom Knows Best: The Universality of
853 Maternal Microbial Transmission. *PLOS Biol* **11**: e1001631.
854 Gill, S.R., Pop, M., Deboy, R.T., Eckburg, P.B., Turnbaugh, P.J., Samuel, B.S., et al. (2006)
855 Metagenomic analysis of the human distal gut microbiome. *Science* **312**: 1355–1359.
856 Gruber-Vodicka, H.R., Seah, B.K.B., and Pruesse, E. (2020) phyloFlash: Rapid Small-
857 Subunit rRNA Profiling and Targeted Assembly from Metagenomes. *mSystems* **5**:.
858 Heimeier, R.A., Das, B., Buchholz, D.R., Fiorentino, M., and Shi, Y.-B. (2010) Studies on
859 Xenopus laevis intestine reveal biological pathways underlying vertebrate gut adaptation from
860 embryo to adult. *Genome Biol* **11**: R55.
861 Hird, S.M. (2017) Evolutionary Biology Needs Wild Microbiomes. *Front Microbiol* **8**: 725.
862 Hofmann, A.F., Hagey, L.R., and Krasowski, M.D. (2010) Bile salts of vertebrates: structural
863 variation and possible evolutionary significance. *J Lipid Res* **51**: 226–246.
864 Hourdry, J., L'Hermite, A., and Ferrand, R. (1996) Changes in the Digestive Tract and
865 Feeding Behavior of Anuran Amphibians during Metamorphosis. *Physiol Zool* **69**: 219–251.
866 Joyce, S.A., MacSharry, J., Casey, P.G., Kinsella, M., Murphy, E.F., Shanahan, F., et al.
867 (2014) Regulation of host weight gain and lipid metabolism by bacterial bile acid
868 modification in the gut. *Proc Natl Acad Sci U S A* **111**: 7421–7426.
869 Kang, D.D., Li, F., Kirton, E., Thomas, A., Egan, R., An, H., and Wang, Z. (2019) MetaBAT
870 2: an adaptive binning algorithm for robust and efficient genome reconstruction from
871 metagenome assemblies. *PeerJ* **7**: e7359.
872 Kohl, K.D., Cary, T.L., Karasov, W.H., and Dearing, M.D. (2013) Restructuring of the
873 amphibian gut microbiota through metamorphosis. *Environ Microbiol Rep* **5**: 899–903.
874 Laczny, C.C., Sternal, T., Plugaru, V., Gawron, P., Atashpendar, A., Margossian, H.H., et al.
875 (2015) VizBin - an application for reference-independent visualization and human-augmented
876 binning of metagenomic data. *Microbiome* **3**: 1.
877 Long, J., Xiang, J., He, T., Zhang, N., and Pan, W. (2020) Gut microbiota differences during
878 metamorphosis in sick and healthy giant spiny frogs (Paa spinosa) tadpoles. *Lett Appl*
879 *Microbiol* **70**: 109–117.
880 Loudon, A.H., Woodhams, D.C., Parfrey, L.W., Archer, H., Knight, R., McKenzie, V., and
881 Harris, R.N. (2014) Microbial community dynamics and effect of environmental microbial
882 reservoirs on red-backed salamanders (Plethodon cinereus). *ISME J* **8**: 830–840.
883 Magnúsdóttir, S., Ravcheev, D., de Crécy-Lagard, V., and Thiele, I. (2015) Systematic
884 genome assessment of B-vitamin biosynthesis suggests co-operation among gut microbes.
885 *Front Genet* **6**:.
886 Mashoof, S., Goodroe, A., Du, C.C., Eubanks, J.O., Jacobs, N., Steiner, J.M., et al. (2013)
887 Ancient T-Independence of Mucosal IgX/A: Gut Microbiota Unaffected by Larval
888 Thymectomy in Xenopus laevis. *Mucosal Immunol* **6**: 358–368.
889 McLaren, M.R., Willis, A.D., and Callahan, B.J. (2019) Consistent and correctable bias in
890 metagenomic sequencing experiments. *eLife* **8**: e46923.
891 Menzel, P., Ng, K.L., and Krogh, A. (2016) Fast and sensitive taxonomic classification for

metagenomics with Kaiju. *Nat Commun* **7**: 11257.
Metchnikoff, O. (1901) Notes sur l'influence des microbes dans le développement des têtards. *Ann Inst Pasteur* **15**: 631–634.
Mikheenko, A., Saveliev, V., and Gurevich, A. (2016) MetaQUAST: evaluation of metagenome assemblies. *Bioinformatics* **32**: 1088–1090.
Moro, E. (1905) Morphologische und biologische Untersuchungen über die Darmbakterien des Säuglings. IV. Der Schottelius's sche Versuch am Kalt- blutler. *Jahrb Kinderheilk* **62**: 467–478.
Naitoh, T., Wassersug, R.J., and Leslie, R.A. (1989) The Physiology, Morphology, and Ontogeny of Emetic behavior in Anuran amphibians. *Physiol Zool* **62**: 819–843.
Narayan, E.J. (2013) Non-invasive reproductive and stress endocrinology in amphibian conservation physiology. *Conserv Physiol* **1**: cot011.
Narayanasamy, S., Jarosz, Y., Muller, E.E.L., Heintz-Buschart, A., Herold, M., Kaysen, A., et al. (2016) IMP: a pipeline for reproducible reference-independent integrated metagenomic and metatranscriptomic analyses. *Genome Biol* **17**: 260.
Pasquier, L.D. (2014) The Development of the Immune System in Xenopus. In *Xenopus Development*. Kloc, lgorzata and Kubiak, J.Z. (eds). John Wiley & Sons, Inc, pp. 264–292.
Peng, Y., Leung, H.C.M., Yiu, S.M., and Chin, F.Y.L. (2012) IDBA-UD: a de novo assembler for single-cell and metagenomic sequencing data with highly uneven depth. *Bioinforma Oxf Engl* **28**: 1420–1428.
Pericard, P., Dufresne, Y., Couderc, L., Blanquart, S., and Touzet, H. (2018) MATAM: reconstruction of phylogenetic marker genes from short sequencing reads in metagenomes. *Bioinformatics* **34**: 585–591.
Pollock, J., Glendinning, L., Wisedchanwet, T., and Watson, M. (2018) The Madness of Microbiome: Attempting To Find Consensus "Best Practice" for 16S Microbiome Studies. *Appl Environ Microbiol* **84**:.
Pryor, G.S. and Bjorndal, K.A. (2005) Symbiotic fermentation, digesta passage, and gastrointestinal morphology in bullfrog tadpoles (Rana catesbeiana). *Physiol Biochem Zool* **78**: 201–215.
R Core Team (2019) R: A language and environment for statistical computing.
Rebollar, E.A. and Harris, R.N. (2019) Editorial: Ecology of Amphibian-Microbial Symbioses. *Front Microbiol* **10**:.
Reschly, E.J., Ai, N., Ekins, S., Welsh, W.J., Hagey, L.R., Hofmann, A.F., and Krasowski, M.D. (2008) Evolution of the bile salt nuclear receptor FXR in vertebrates. *J Lipid Res* **49**: 1577–1587.
Ridlon, J.M., Kang, D.J., Hylemon, P.B., and Bajaj, J.S. (2014) Bile Acids and the Gut Microbiome. *Curr Opin Gastroenterol* **30**: 332–338.
Robert, J. and Ohta, Y. (2009) Comparative and developmental study of the immune system in Xenopus. *Dev Dyn* **238**: 1249–1270.
Rollins-Smith, L.A., Barker, K.S., and Davis, A.T. (1997) Involvement of glucocorticoids in the reorganization of the amphibian immune system at metamorphosis. *Dev Immunol* **5**: 145–152.
Sachs, L.M. and Buchholz, D.R. (2019) Insufficiency of Thyroid Hormone in Frog Metamorphosis and the Role of Glucocorticoids. *Front Endocrinol* **10**: 287.
Saengkerdsub, S. and Ricke, S.C. (2014) Ecology and characteristics of methanogenic archaea in animals and humans. *Crit Rev Microbiol* **40**: 97–116.
Schreiber, A.M., Cai, L., and Brown, D.D. (2005) Remodeling of the intestine during metamorphosis of Xenopus laevis. *Proc Natl Acad Sci U S A* **102**: 3720–3725.
Seemann, T. (2014) Prokka: rapid prokaryotic genome annotation. *Bioinforma Oxf Engl* **30**: 2068–2069.

942 Sekirov, I., Russell, S.L., Antunes, L.C.M., and Finlay, B.B. (2010) Gut microbiota in health
943 and disease. *Physiol Rev* **90**: 859–904.
944 Seo, Y.-W., Sanyal, S., Kim, H.-J., Won, D.H., An, J.-Y., Amano, T., et al. (2002) FOR, a
945 Novel Orphan Nuclear Receptor Related to Farnesoid X Receptor. *J Biol Chem* **277**: 17836–
946 17844.
947 Shenhav, L., Thompson, M., Joseph, T.A., Briscoe, L., Furman, O., Bogumil, D., et al. (2019)
948 FEAST: fast expectation-maximization for microbial source tracking. *Nat Methods* **16**: 627–
949 632.
950 Sieber, C.M.K., Probst, A.J., Sharrar, A., Thomas, B.C., Hess, M., Tringe, S.G., and Banfield,
951 J.F. (2018) Recovery of genomes from metagenomes via a dereplication, aggregation and
952 scoring strategy. *Nat Microbiol* **3**: 836–843.
953 Sommer, F. and Bäckhed, F. (2013) The gut microbiota--masters of host development and
954 physiology. *Nat Rev Microbiol* **11**: 227–238.
955 Song, Z., Cai, Y., Lao, X., Wang, X., Lin, X., Cui, Y., et al. (2019) Taxonomic profiling and
956 populational patterns of bacterial bile salt hydrolase (BSH) genes based on worldwide human
957 gut microbiome. *Microbiome* **7**: 9.
958 Uritskiy, G.V., DiRuggiero, J., and Taylor, J. (2018) MetaWRAP—a flexible pipeline for
959 genome-resolved metagenomic data analysis. *Microbiome* **6**: 158.
960 Vences, M., Lyra, M.L., Kueneman, J.G., Bletz, M.C., Archer, H.M., Canitz, J., et al. (2016)
961 Gut bacterial communities across tadpole ecomorphs in two diverse tropical anuran faunas.
962 *Naturwissenschaften* **103**: 25.
963 Vouillot, L., Thélie, A., Scalvenzi, T., and Pollet, N. (2014) Genomics and Genome
964 Engineering in Xenopus. In *Xenopus Development*. Kloc, lgorzata and Kubiak, J.Z. (eds).
965 John Wiley & Sons, Inc, pp. 383–402.
966 Wahlström, A., Sayin, S.I., Marschall, H.-U., and Bäckhed, F. (2016) Intestinal Crosstalk
967 between Bile Acids and Microbiota and Its Impact on Host Metabolism. *Cell Metab* **24**: 41–
968 50.
969 Walke, J.B., Becker, M.H., Loftus, S.C., House, L.L., Cormier, G., Jensen, R.V., and Belden,
970 L.K. (2014) Amphibian skin may select for rare environmental microbes. *ISME J* **8**: 2207–
971 2217.
972 Warne, R.W., Kirschman, L., and Zeglin, L. (2019) Manipulation of gut microbiota during
973 critical developmental windows affects host physiological performance and disease
974 susceptibility across ontogeny. *J Anim Ecol* **88**: 845–856.
975 Warne, R.W., Kirschman, L., and Zeglin, L. (2017) Manipulation of Gut Microbiota Reveals
976 Shifting Community Structure Shaped by Host Developmental Windows in Amphibian
977 Larvae. *Integr Comp Biol* **57**: 786–794.
978 Watanabe, M., Houten, S.M., Mataki, C., Christoffolete, M.A., Kim, B.W., Sato, H., et al.
979 (2006) Bile acids induce energy expenditure by promoting intracellular thyroid hormone
980 activation. *Nature* **439**: 484–489.
981 Wilson, D.S. and Sober, E. (1989) Reviving the superorganism. *J Theor Biol* **136**: 337–356.
982 Wollman, E. (1913) Sur l'élevage des têtards stériles. *Ann Inst Pasteur* **27**: 154–161.
983 Wollman, E. and Wollman, E. (1915) Les microbes dans l'alimentation des têtards. *Compte-*
984 *Rendu Société Biol* **78**: 195–197.
985 Wood, D.E., Lu, J., and Langmead, B. (2019) Improved metagenomic analysis with Kraken 2.
986 *Genome Biol* **20**: 257.
987 Wu, Y.-W., Simmons, B.A., and Singer, S.W. (2016) MaxBin 2.0: an automated binning
988 algorithm to recover genomes from multiple metagenomic datasets. *Bioinforma Oxf Engl* **32**:
989 605–607.
990 Ye, Y. and Doak, T.G. (2009) A Parsimony Approach to Biological Pathway
991 Reconstruction/Inference for Genomes and Metagenomes. *PLOS Comput Biol* **5**: e1000465.

992 Youngblut, N.D., Reischer, G.H., Walters, W., Schuster, N., Walzer, C., Stalder, G., et al.
993 (2019) Host diet and evolutionary history explain different aspects of gut microbiome
994 diversity among vertebrate clades. *Nat Commun* **10**: 2200.
995 Zhang, M., Chen, H., Liu, L., Xu, L., Wang, X., Chang, L., et al. (2020) The Changes in the
996 Frog Gut Microbiome and Its Putative Oxygen-Related Phenotypes Accompanying the
997 Development of Gastrointestinal Complexity and Dietary Shift. *Front Microbiol* **11**: 162.
998 Zilber-Rosenberg, I. and Rosenberg, E. (2008) Role of microorganisms in the evolution of
999 animals and plants: the hologenome theory of evolution. *FEMS Microbiol Rev* **32**: 723–735.
1000

1001 # Figure legends

1002 **Figure 1**: **Cytometric profiles of gut bacteria during *Xenopus tropicalis* development.**

1003 **A. Cytometric profiles**. Each dot in the plot represents one event (i.e. a cell), the color
1004 represents the density of overlapping point from red (low) to blue (high). The vertical axis
1005 represents DNA content by the measurement of propidium iodide (PI) fluorescence (614/20nm)
1006 and the horizontal axis represents relative cell size by the measurement of forward scatter.
1007 Different bacterial populations are highlighted by an ellipse and identified by a text label. Top-
1008 right events labelled with a "b" correspond to the beads used for normalization. Background
1009 signals have been removed. **B. Enumeration of bacterial load during development**. The
1010 vertical axis represents the number of bacteria and the horizontal axis corresponds to different
1011 stages of development. Each dot corresponds to a biological replicate, the error bar represents
1012 the standard deviation obtained by technical replicates. A ★ marks the beginning of feeding
1013 and ★★ marks the change from the tadpole to the adult diet.

1014 **Figure 2: Phylum and Family-level compositional changes in the Xenopus gut microbiome**
1015 **across development.**

1016 **A.** Bar plot representation of bacterial diversity at the phylum level. Results for the different
1017 life stages studied are shown in the following order, from top to bottom: Premetamorphic
1018 tadpoles (NF54 to NF56); Prometamorphic tadpoles (NF58 to NF61); Metamorphic tadpole

1019 (NF 62); Froglet (NF66); Adult: sexually mature adults (males and females). B. Bar plot
1020 representation of bacterial diversity at the family level, in the same order as A. C. Same as A
1021 but viewed at the sample level to highlight interindividual differences. D. Bar plot
1022 representation of Gram-positive and Gram-negative bacterial phyla.

1023 **Figure 3: *Xenopus* microbiota across several adult organs and samples**

1024 **A.** Bar plot representation of bacterial diversity at the phylum level. **B.** Principal coordinate
1025 analysis of microbial communities across several adult organs and samples. Community
1026 membership was analyzed using unweighted UniFrac distance, and community structure was
1027 analyzed using weighted UniFrac distance. Percentages of the explained variations are
1028 indicated on both axes.

1029 **Figure 4: Prevalence and abundances of active bacteria across Xenopus development**
1030 **from post-hatching to metamorphosis.**

1031 **A.** Heatmap of prevalence and abundances for 33 OTUs. The detection threshold scale is
1032 logarithmic and the metric used was the relative abundance. OTUs were identified using their
1033 taxonomic affiliation at the family genus or species level according to the resolution available
1034 for a given OTU. This analysis was performed on OTUs characterized by a minimal prevalence
1035 of 50 % and a minimal abundance of 0.001%.

1036 **B.** Abundance heatmap for the 33 most prevalent OTUs across the developmental stages
1037 sampled. Two clutches were followed up across development, and the white dotted lines
1038 separate the two biological replicate samples. The legend for stages is as follows: PE is a post-
1039 hatching NF30 tailbud embryonic stage; NF41 is a premetamorphic tadpole non-feeding stage;
1040 NF48 is a premetamorphic tadpole feeding stage; NF50; NF 52 and NF56 are premetamorphic
1041 tadpole feeding stages; NF60 is a prometamorphic tadpole stage; NF63 are metamorphic
1042 tadpole stages; NF66 is a froglet stage.

1043 **Figure 5: Influence of tadpole's diet on their gut microbiome.**

1044 A. Bar plot representation of bacterial diversity at the phylum level. B. Principal coordinate
1045 analysis of microbial communities across several adult organs and samples. Community
1046 membership was analyzed using unweighted UniFrac distance, and community structure was
1047 analyzed using weighted UniFrac distance. Percentages of the explained variations are
1048 indicated on both axes. Tadpole Food 1 (D1 samples) was a micro planktonic-based diet and
1049 tadpole food 2 (D2 samples) (food 1) was a sterile flour.

1050 **Figure 6: *X. tropicalis* microbiome transmission**

1051 A. Bar plot representation of bacterial diversity at the phylum level.

1052 B. Box-plot representation of weighted UniFrac distances between eggs, skin and feces. Letters
1053 a, b and c indicate significant differences at the 0.05 level between or within samples according
1054 to pairwise Dunn's rank sum post-hoc test (see Methods section for details). Note the outliers
1055 in the feces sample and in the eggs-skin comparison.

1056 C. Bar plot representation of source proportions in egg microbiomes.

1057 D. Principal coordinate analysis of microbial communities across eggs, feces and skin samples.
1058 Community composition was analyzed using PhilR distance. Percentages of explained
1059 variations are indicated on both axes.

1060 **Figure 7**: **Bacterial taxonomic profiles from *X. tropicalis* prometamorphic tadpole gut.**

1061 A. Histogram representation of bacterial diversity at the phylum level observed in a pool of five
1062 prometamorphic tadpole's guts at stage NF56. metaDNA: metagenomic analysis; metaRNA:
1063 metatranscriptomic analysis. Each color in the histogram refers to a phylum as described in the
1064 legend. B. Vizualisation of the metagenomic assembly. Each bin identified using DASTool is
1065 represented in a different colour, each circle is a contig. The circles diameter is proportional to
1066 contig length.

1067 **Figure 8**: **Overview of *X. tropicalis* tadpole's microbiota metabolic functions. A.** This
1068 barplot represents the read coverage (x-axis, in transcripts per kilobase million) on genes

1069 encoding enzymes participating in various Metacyc pathways (y-axis). **B.** Counts of
1070 metagenome bins, genes and scaffolds in which enzymes involved in selected biosynthetic
1071 pathways. Expressed genes encoding enzymes involved in selected KEGG modules mentioned
1072 on the y-axis were counted.
1073
1074 **Supplementary data R scripts: R markdown rendered html files are available at**
1075 **https://npollet.github.io/metatetard**
1076
1077 **Additional files:**
1078 **Additional file 1: Supplementary_table_1.csv**
1079 File format: csv
1080 Title of data: Metadata.
1081 Description of data: This file contains the metadata corresponding to samples analysed by 16S
1082 rRNA gene metabarcoding.
1083
1084 **Additional file 2: Supplementary_table_2**
1085 File format: xlsx
1086 Title of data: Compilation of statistical results in tables.
1087 Description of data: This file contains seven tables compiling the results of significance tests
1088 for alpha and beta diversity metrics.
1089
1090 **Additional file 3: Figure_S1**
1091 File format: pdf
1092 Title of data: Microbial cell populations identified by flow cytometry across developmental
1093 stages.

1094 Description of data: Cytometric profiles obtained at different stages of tadpole's development
1095 were used to identify visually bacterial populations. Each population was plotted according to
1096 its DNA content and relative size (error bars correspond to the standard error deviation).
1097 Vertical axis represents the measurement of fluorescence (propidium iodide - 614/20nm) and
1098 the horizontal axis the measurement of relative cell size (forward scatter, in arbitrary units).
1099 The bacterial populations clearly corresponding across life stages are grouped by a dotted
1100 ellipse.
1101
1102
1103 **Additional file 4: Figure_S2**
1104 File format: pdf
1105 Title of data: Rarefaction and species accumulation curves.
1106 Description of data: These graphs present rarefaction curves (top) and species accumulation
1107 curves (bottom) for the different samples used in the listed experiments. * For premetamorph
1108 samples, the rarefaction curve is shown only up to 60,000 reads for the sake of consistency
1109 between all plots. Species richness corresponds to OTUs number. A detailed analysis is
1110 presented at https://npollet.github.io/metatetard/xpall_rarefaction_phyloseq.html
1111
1112
1113
1114 **Additional file 5: Figure_S3**
1115 File format: pdf
1116 Title of data: Bacterial communities in the *Xenopus* gut across development.
1117 Description of data:

1118 A. Graphical representation of the bacterial species richness. Each point corresponds to the
1119 breakaway richness estimate, error bars represent the measurement error according to the
1120 breakaway model. Premet: premetamorphic tadpoles NF54 to NF56. Promet: prometamorphic
1121 tadpoles NF58 to NF61; Meta: Metamorphic tadpole NF 62; Fro: Froglet NF66; Adult: sexually
1122 mature adults. Horizontal lines represent significant differences between the life stages
1123 connected; p=0.000 both between Premet. and Promet. and between Premet. and Adult. B.
1124 Representation of the bacterial species diversity measured using the Shannon index. Each large
1125 point corresponds to the divnet Shannon estimate from the samples of the same life stage, error
1126 bars represent the measurement error. Each small point corresponds to the divnet Shannon
1127 estimate from a given sample. The error bar corresponding to the measurement error can not be
1128 seen at this scale. Horizontal lines represent significant differences between the life stages
1129 connected; p=0.000 in all significant cases including the global test (p=0.875 for Premet-Meta).
1130 C. Principal coordinate analysis of gut-associated microbial communities during Xenopus
1131 development. Community membership was analyzed using unweighted Unifrac distance, and
1132 community composition was analyzed using philR distance. Percentages of the explained
1133 variations are indicated on both axes.
1134
1135
1136 **Additional file 6: Figure_S4**
1137 File format: pdf
1138 Title of data: Shared and contrasting bacterial communities in the Xenopus gut microbiome
1139 across development.
1140 Description of data: A : Venn diagram showing the number of shared OTUs between samples
1141 of the same developmental stage category. B : Bar plot of the total number of OTUs in each
1142 developmental stage category. C : Number of shared and specific OTUs. D : Heatmap plot of

1143 the prevalence and abundances for low-abundance OTUs. The detection threshold scale is
1144 logarithmic and the metric used was the relative abundance. This analysis was performed on
1145 OTUs characterized by a minimal prevalence of 50 % and a minimal abundance of 1e-5 %. E.
1146 Prevalence and abundances of the most common and the most abundant OTUs across
1147 development. OTUs were identified using their taxonomic affiliation at the family genus or
1148 species level according to the resolution available for a given OTU. This analysis was
1149 performed on OTUs characterized by a minimal prevalence of 50 % and a minimal abundance
1150 of 0.001%. The right panel shows an abundance heatmap for the same OTUs to visualize their
1151 abundances in each sample.
1152
1153 **Additional file 7: Figure_S5**
1154 File format: pdf
1155 Title of data: Contrasting OTUs across development
1156 Description of data: A : Abundance fold changes across development. Contrasting OTUs were
1157 identied by filtering OTUs with an abundance of at least 100 reads across 20% of sample and
1158 using DEseq2 with a significance cutoff of 0.01. B : Heatmap representation of contrasting
1159 OTUs abundances across development. The heatmap was produced using a principal
1160 component analysis based on UniFrac distances.
1161
1162 **Additional file 8: Figure_S6**
1163 File format: pdf
1164 Title of data: Variations of the phylogenetic structure of the *Xenopus* gut microbiota during
1165 development.
1166 Description of data: Standardized effect sizes of the Mean pairwise distance (left panel) and of
1167 the mean nearest taxon distance (right panel) measured using Faith' PD index for *X. tropicalis*

1168 gut microbial communities across developmental life stages as indicated on the x-axis. Letters
1169 a, b and c indicate significant differences at the 0.05 level between developmental stages
1170 according to pairwise Dunn's rank sum post-hoc test (see Methods section for details).
1171
1172 **Additional file 9: Figure_S7**
1173 File format: pdf
1174 Title of data: *Xenopus* tadpole active bacterial communities: alpha-diversity, bacterial phylum
1175 diversity and source proportions
1176 Description of data: A : Bar plot representation of OTU richness and phylogenetic diversity in
1177 active bacterial communities. Two clutches were followed up across early development, and
1178 the light and dark grey bars correspond to the two biological replicate samples. The legend for
1179 stages is as follows: NF30 is a post-hatching tailbud embryonic stage; NF41 is a
1180 premetamorphic tadpole non-feeding stage; NF48 is a premetamorphic tadpole feeding stage;
1181 NF50 and NF 52 are premetamorphic tadpole feeding stages. B : Bar plot representation of the
1182 bacterial phylum diversity. C : Bar plot representation of source proportions in froglet gut
1183 microbiome. Abbreviations SL and TGA refer to *X. tropicalis* strain's names : SL for Sierra
1184 Leone strain and TGA for a laboratory population of Adiopodoume strain (Ivory Coast) outbred
1185 to Uyere strain (Nigeria).
1186
1187 **Additional file 10: Figure_S8**
1188 File format: pdf
1189 Title of data: Impact of the food regime on tadpole growth and development.
1190 Description of data: A: Impact of food diet on tadpole growth and development. Tadpoles were
1191 fed using either a micro planktonic-based diet (food 1) or a sterile flour (food 2). Their growth
1192 was assessed by weighting them, and their development was monitored by assessing their

1193 developmental stage according to the Nieuwkoop and Faber developmental table. The food
1194 regime did not change significantly tadpole growth (Kruskal-Wallis chi-squared = 0.99, df = 1,
1195 p = 0.32) or development (Kruskal-Wallis chi-squared = 0.34, df = 1, p = 0.56). B : Impact of
1196 the food regime on tadpole's guts microbial communities. These bar plot shows values of the
1197 Standardized effect size of the Mean Pairwise Distance (SES MPD) and of the Mean Nearest
1198 Taxon Distance (SES MNTD) according to the food regime given to groups of tadpoles. The
1199 result of a Wilcoxon signed-rank test is shown above the graphs, with W being the Wilcoxon
1200 test statistic computed by this test, p the p-value, r the effect size, CI the confidence interval of
1201 the effect size and n the number of observations (see
1202 https://indrajeetpatil.github.io/statsExpressions/). C : Abundance ratios of the OTUs found
1203 significantly different according to a change of diet.
1204

1205 **Additional file 11: Figure_S9**

1206 File format: html

1207 Title of data: Krona plot view of taxonomic affiliations inferred from a MATAM assembly of
1208 *X. tropicalis* tadpole's gut metagenomic reads.

1209 Description of data: *X. tropicalis* tadpole's gut metagenomic reads were used as input for the
1210 identification and assembly of SSU rRNA sequences using MATAM. Taxonomic affiliations
1211 were then inferred using SILVA
1212

1213 **Additional file 12: Figure_S10**

1214 File format: html

1215 Title of data: Results of a phyloFlash assembly of *X. tropicalis* tadpole's gut metagenomic
1216 reads.

1217 Description of data: *X. tropicalis* tadpole's gut metagenomic reads were used as input for the
1218 identification and assembly of LSU and SSU rRNA sequences using phyloFlash. The results
1219 for Spades and Emirge assembly engines are shown. Taxonomic affiliations were then inferred
1220 using SILVA
1221
1222 **Additional file 13: Figure_S11**
1223 File format: html
1224 Title of data: Krona plot view of taxonomic affiliations inferred from a MATAM assembly of
1225 *X. tropicalis* tadpole's gut metatranscriptomic reads.
1226 Description of data: *X. tropicalis* tadpole's gut metatranscriptomic reads were used as input for
1227 the identification and assembly of SSU rRNA sequences using MATAM. Taxonomic
1228 affiliations were then inferred using SILVA
1229
1230 **Additional file 14: Figure_S12**
1231 File format: html
1232 Title of data: Results of a phyloFlash assembly of *X. tropicalis* tadpole's gut metatranscriptomic
1233 reads.
1234 Description of data: *X. tropicalis* tadpole's gut metatranscriptomic reads were used as input for
1235 the identification and assembly of LSU and SSU rRNA sequences using phyloFlash. The results
1236 for Spades, Emirge and Trinity (trusted contigs) assembly engines are shown. Taxonomic
1237 affiliations were then inferred using SILVA
1238
1239 **Additional file 13: Supplementary table 3**
1240 File format: xlsx
1241 Title of data: Comparison of metagenomic assemblies

1242 Description of data: This file contains the metrics obtained using metaQUAST on different
1243 assemblies of metagenomic reads.
1244
1245 **Additional file 14: Supplementary table 4**
1246 File format: xlsx
1247 Title of data: Results of DASTool binning
1248 Description of data: This file contains the summary of DASTool binning results.
1249
1250 **Additional file 15: Figure_S13**
1251 File format: html
1252 Title of data: Krona plot view of predicted KEGG metabolic pathways.
1253 Description of data: KEGG metabolic pathways were predicted based on Minpath inference
1254 from EC enzyme numbers obtained using prokka.
1255
1256
1257 **Additional file 16: Figure_S14**
1258 File format: html
1259 Title of data: Krona plot view of predicted Metacyc metabolic pathways.
1260 Description of data: Metacyc metabolic pathways were predicted based on Minpath inference
1261 from EC enzyme numbers obtained using prokka.
1262
1263 **Additional file 17: Figure_S15**
1264 File format: pdf
1265 Title of data: Metabolic map of *X. tropicalis* genome and its gut metagenome.

1266 Description of data: This metabolic pathway highlights in green the metabolic pathways
1267 predicted from the *Xenopus* genome and in blue those predicted from the tadpole gut
1268 metagenome. This map can be interactively accessed at
1269 https://pathways.embl.de/selection/pWbci4bo871W8Qm8XKF
1270
1271
1272 **Additional file 18: Figure_S16**
1273 File format: pdf
1274 Title of data: Selected cases of metabolic potential of *X. tropicalis* genome and its gut
1275 metagenome.
1276 Description of data: Fragments of biosynthetic pathways for common short-chain fatty acids,
1277 nitrogen recycling and B-vitamins is depicted.
1278 This metabolic pathway highlights in green the metabolic pathways predicted from the *Xenopus*
1279 genome and in blue those predicted from the tadpole gut metagenome. This map can be
1280 interactively accessed at https://pathways.embl.de/selection/pWbci4bo871W8Qm8XKF
1281
1282 **Additional file 19: Extended_materials_and_methods**
1283 File format: docx
1284 Title of data: Extended materials and methods.
1285 Description of data: This file contains an extended version of the materials and methods
1286

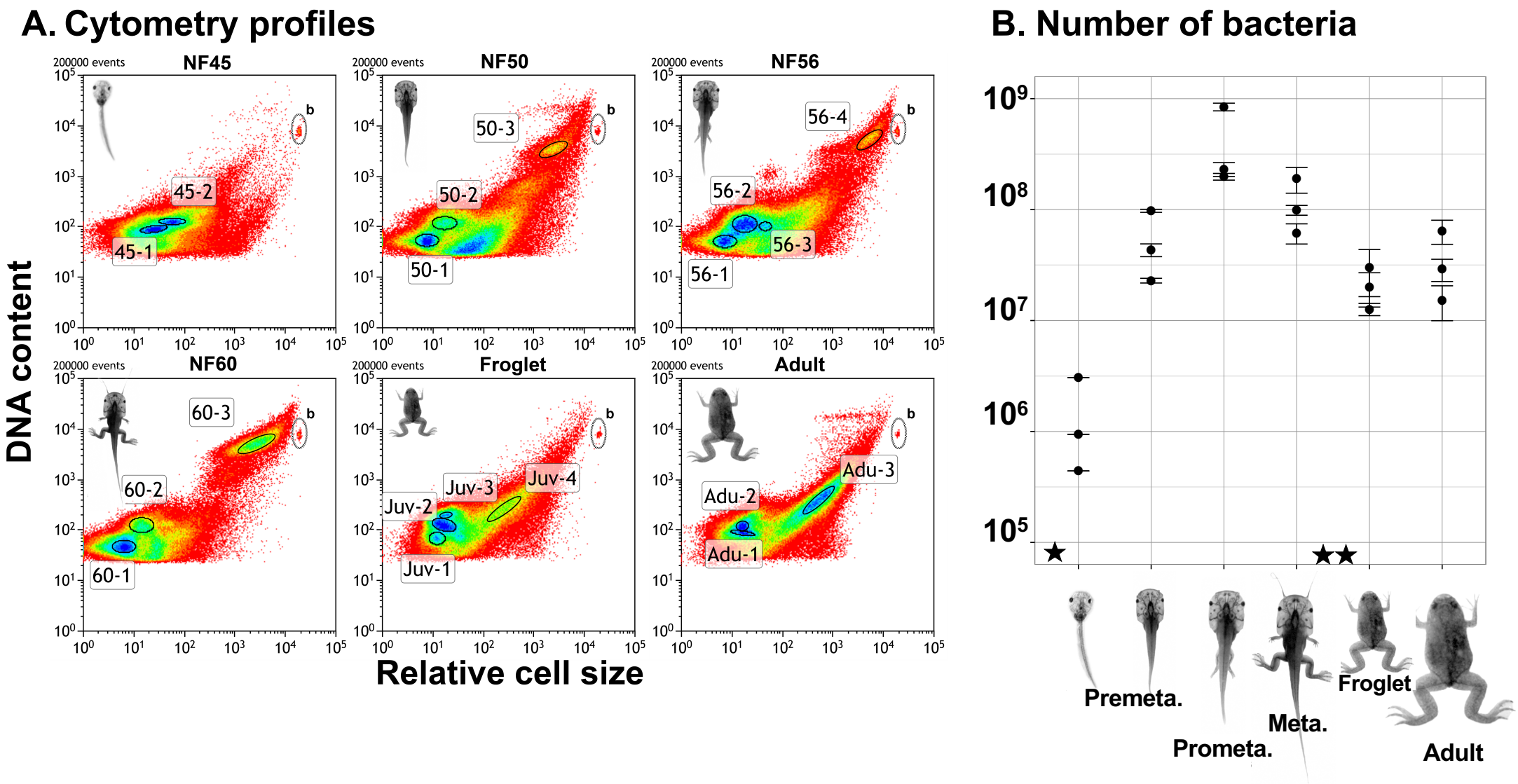

Figure 1. Scalvenzi et al.

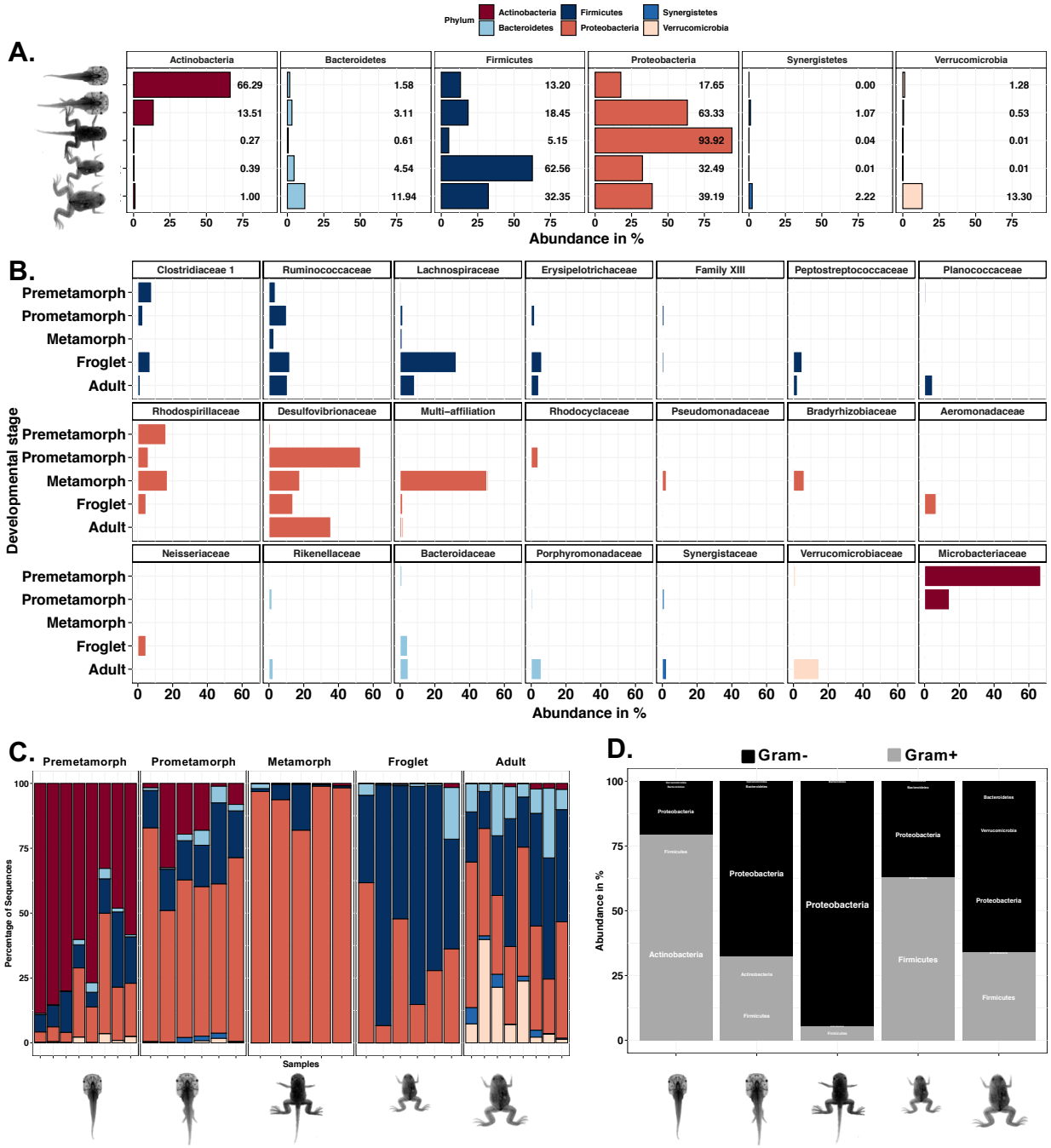

Figure 2. Scalvenzi et al.

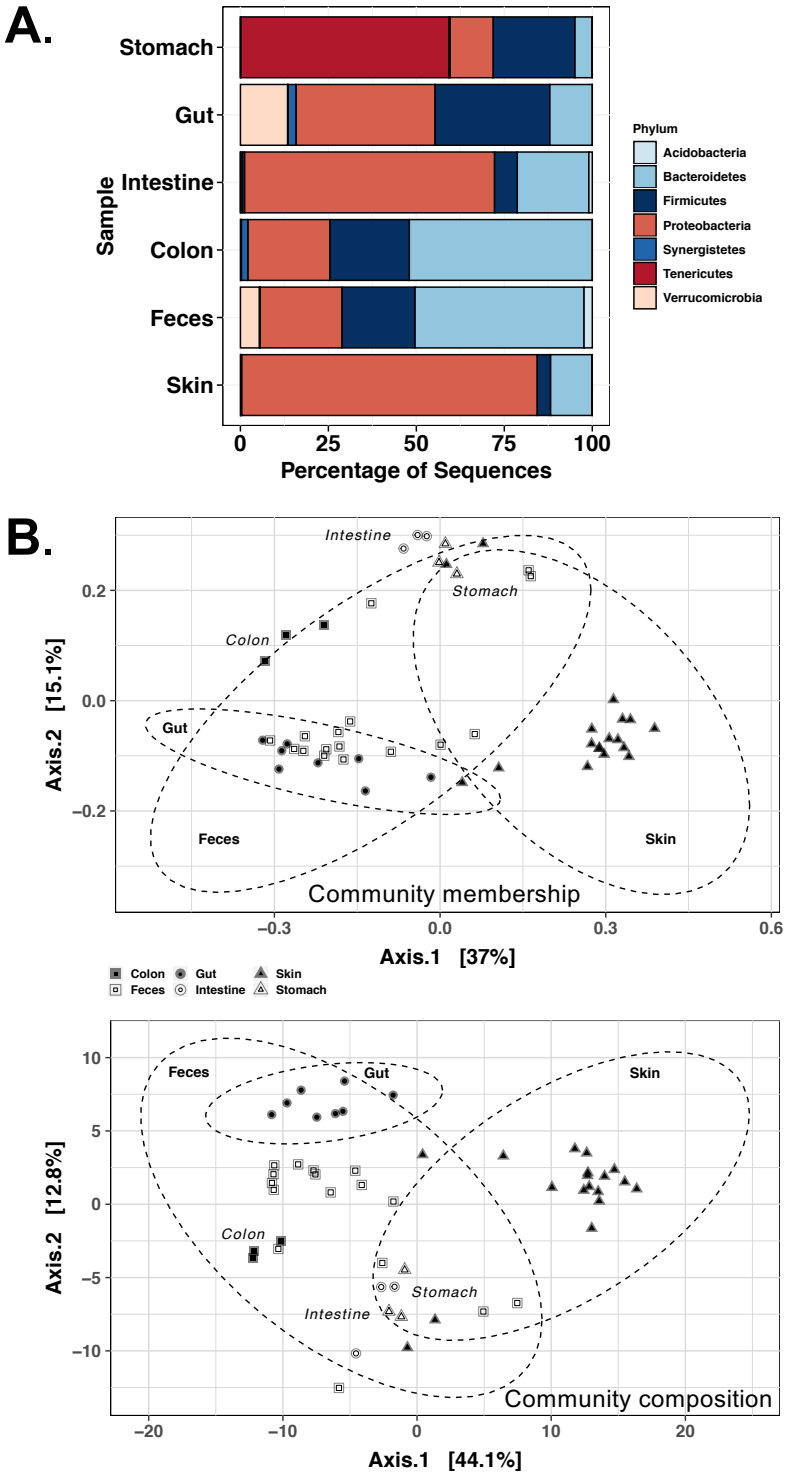

Figure 3. Scalvenzi et al.

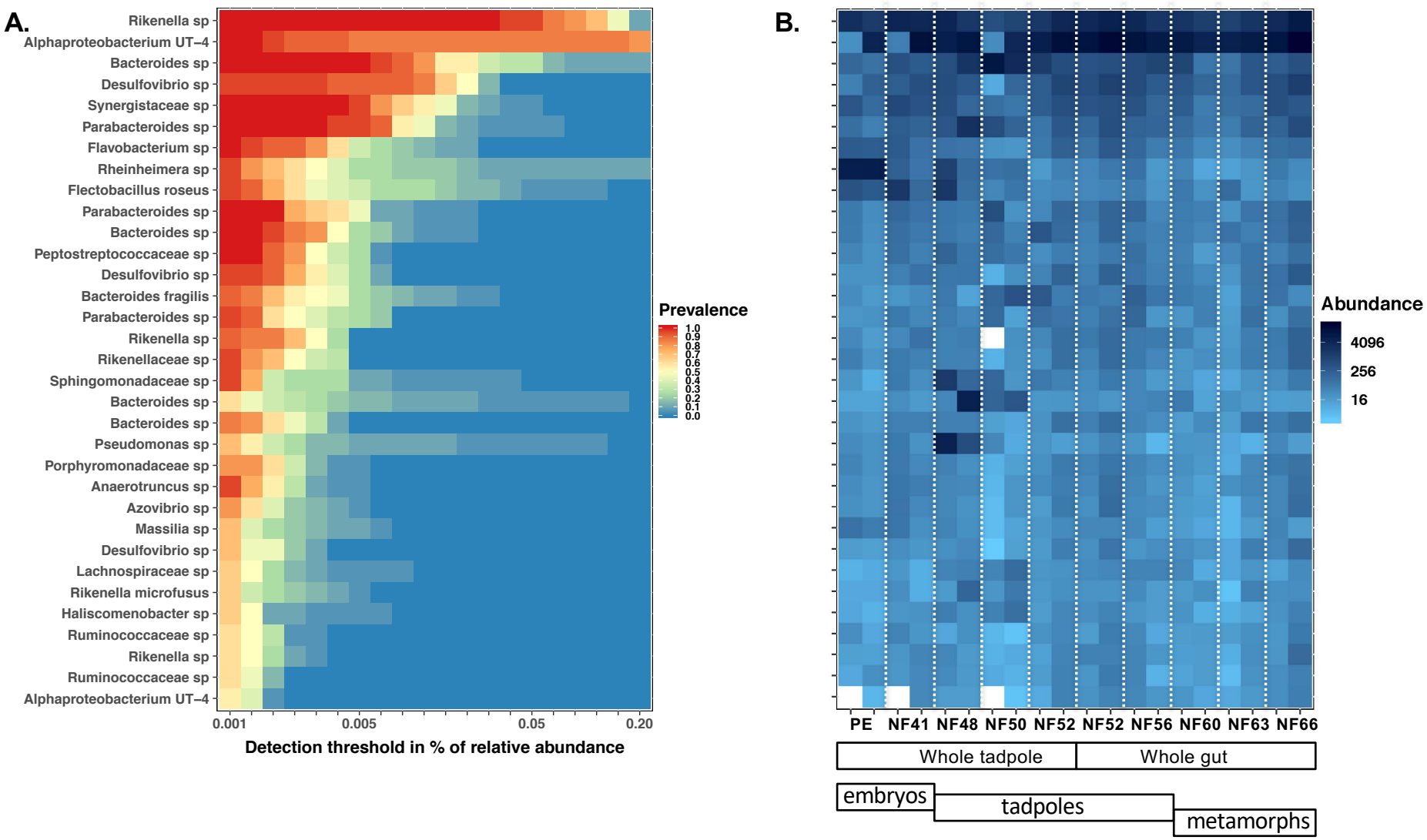

Figure 4. Scalvenzi et al.

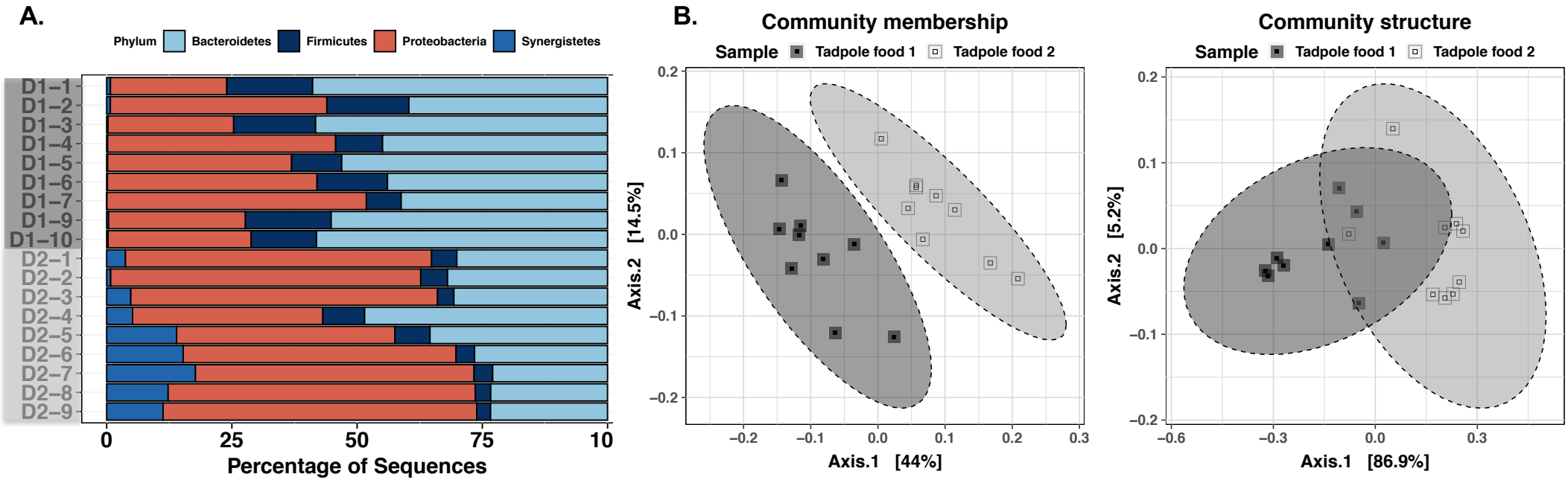

Figure 5. Scalvenzi et al.

Figure 6. Scalvenzi et al.

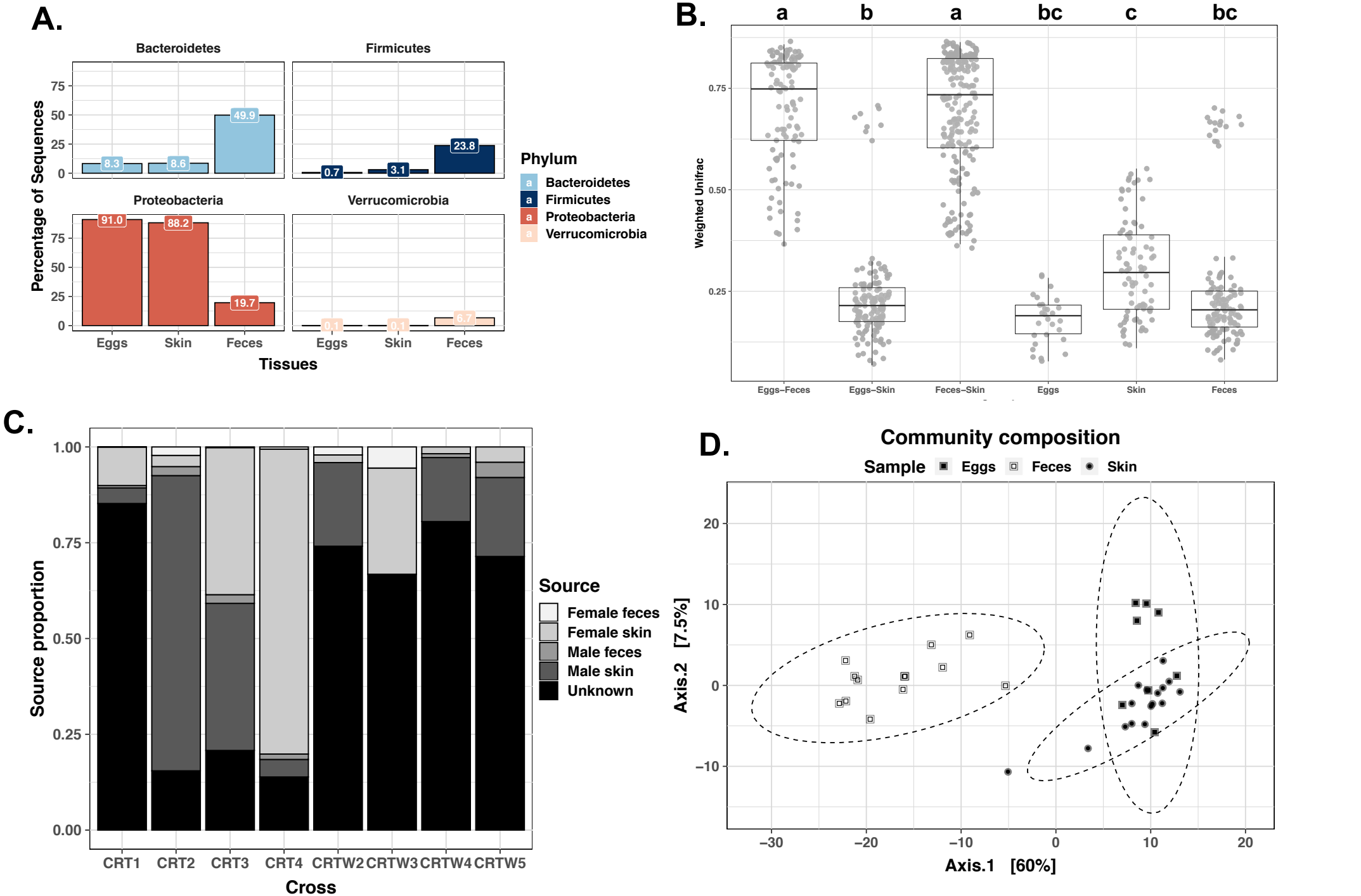

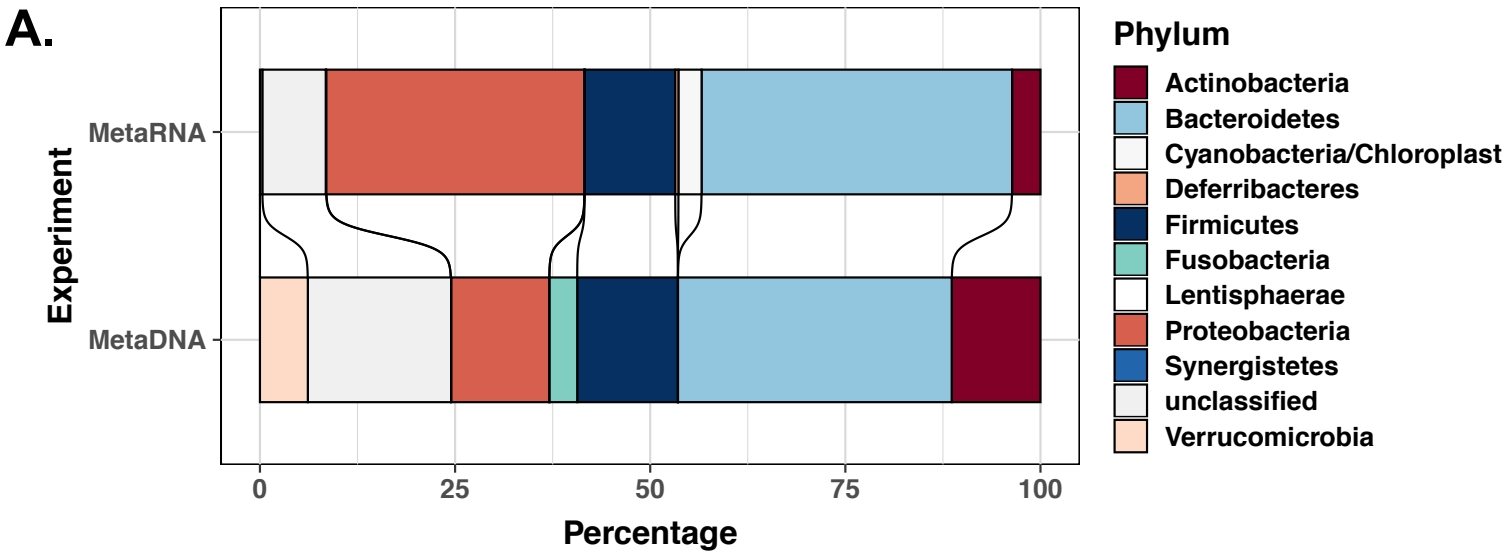

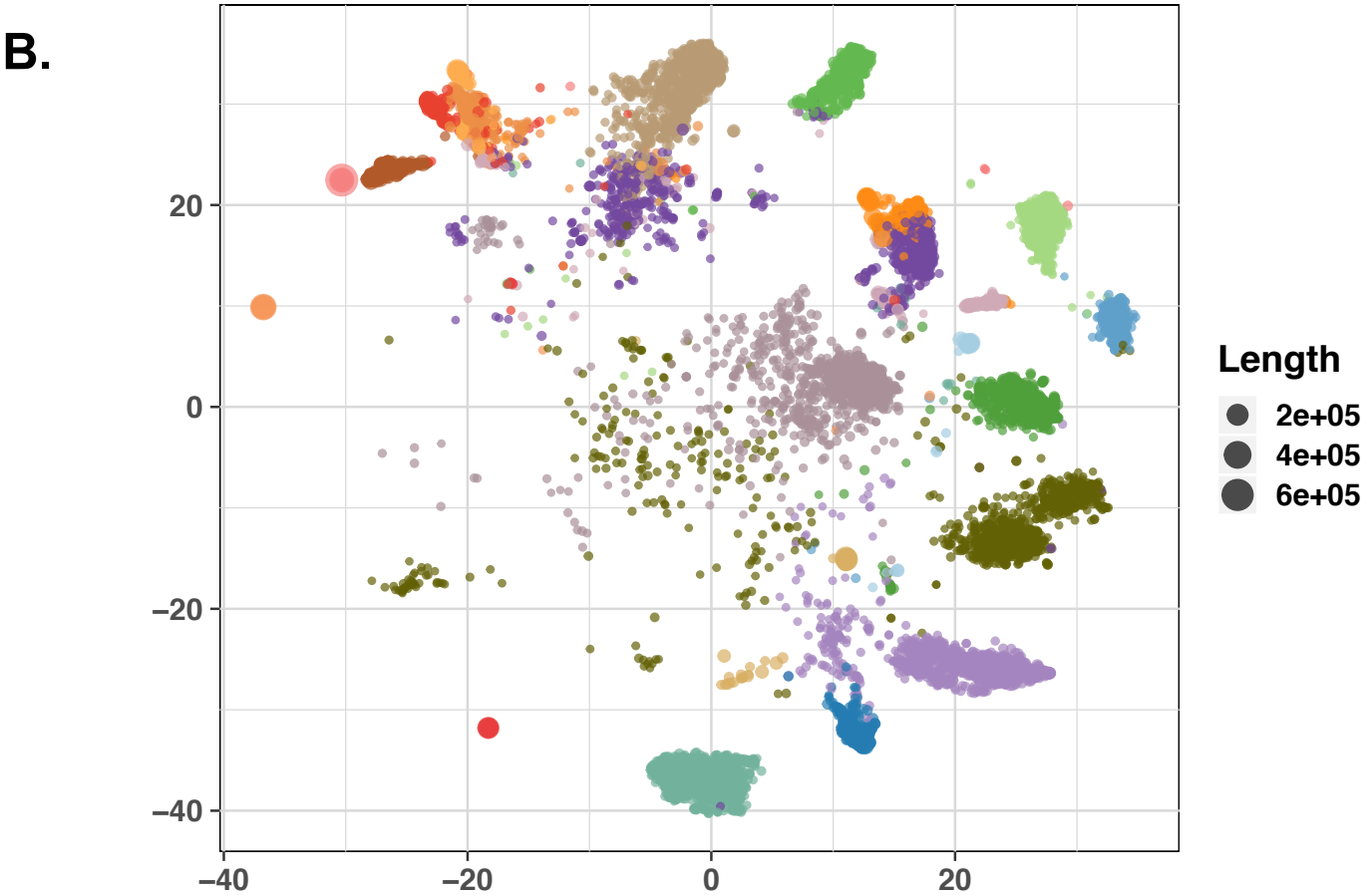

Figure 7. Scalvenzi et al.

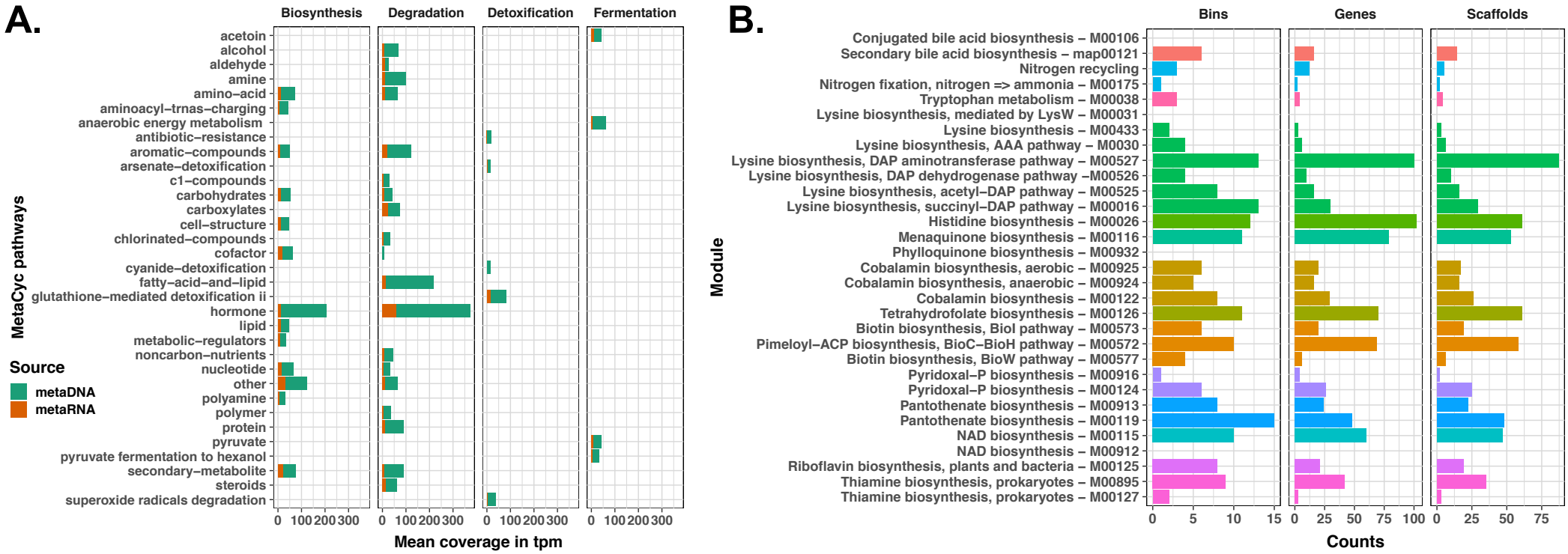

Figure 8. Scalvenzi et al.

Figure 1: Cytometric profiles of gut bacteria during Xenopus tropicalis development.

A. Cytometric profiles. Each dot in the plot represents one event (i.e. a cell), the color represents the density of overlapping point from red (low) to blue (high). The vertical axis represents DNA content by the measurement of propidium iodide (PI) fluorescence (614/20nm) and the horizontal axis represents relative cell size by the measurement of forward scatter. Different bacterial populations are highlighted by an ellipse and identified by a text label. Top-right events labelled with a “b” correspond to the beads used for normalization. Background signals have been removed. B. Enumeration of bacterial load during development. The vertical axis represents the number of bacteria and the horizontal axis corresponds to different stages of development. Each dot corresponds to a biological replicate, the error bar represents the standard deviation obtained by technical replicates. A ★ marks the beginning of feeding and ★★ marks the change from the tadpole to the adult diet.

Figure 2: Phylum and Family-level compositional changes in the Xenopus gut microbiome across development.

A. Bar plot representation of bacterial diversity at the phylum level. Results for the different life stages studied are shown in the following order, from top to bottom: Premetamorphic tadpoles (NF54 to NF56); Prometamorphic tadpoles (NF58 to NF61); Metamorphic tadpole (NF 62); Froglet (NF66); Adult: sexually mature adults (males and females). B. Bar plot representation of bacterial diversity at the family level, in the same order as A. C. Same as A but viewed at the sample level to highlight interindividual differences. D. Bar plot representation of Gram-positive and Gram-negative bacterial phyla.

Figure 3: Xenopus microbiota across several adult organs and samples

A. Bar plot representation of bacterial diversity at the phylum level. B. Principal coordinate analysis of microbial communities across several adult organs and samples. Community membership was analyzed using unweighted UniFrac distance, and community structure was analyzed using weighted UniFrac distance. Percentages of the explained variations are indicated on both axes.

Figure 4: Prevalence and abundances of active bacteria across Xenopus development from post-hatching to metamorphosis.

A. Heatmap of prevalence and abundances for 33 OTUs. The detection threshold scale is logarithmic and the metric used was the relative abundance. OTUs were identified using their taxonomic affiliation at the family genus or species level according to the resolution available for a given OTU. This analysis was performed on OTUs characterized by a minimal prevalence of 50 % and a minimal abundance of 0.001%. B. Abundance heatmap for the 33 most prevalent OTUs across the developmental stages sampled. Two clutches were followed up across development, and the white dotted lines separate the two biological replicate samples. The legend for stages is as follows: PE is a post-hatching NF30 tailbud embryonic stage; NF41 is a premetamorphic tadpole non-feeding stage; NF48 is a premetamorphic tadpole feeding stage; NF50; NF 52 and NF56 are premetamorphic tadpole feeding stages; NF60 is a prometamorphic tadpole stage; NF63 are metamorphic tadpole stages; NF66 is a froglet stage.

Figure 5: Influence of tadpole's diet on their gut microbiome.
A. Bar plot representation of bacterial diversity at the phylum level. B. Principal coordinate analysis of microbial communities across several adult organs and samples. Community membership was analyzed using unweighted UniFrac distance, and community structure was analyzed using weighted UniFrac distance. Percentages of the explained variations are indicated on both axes. Tadpole Food 1 (D1 samples) was a micro planktonic-based diet and tadpole food 2 (D2 samples) (food 1) was a sterile flour.

Figure 6: X. tropicalis microbiome transmission.
A. Bar plot representation of bacterial diversity at the phylum level. B. Box-plot representation of weighted UniFrac distances between eggs, skin and feces. Letters a, b and c indicate significant differences at the 0.05 level between or within samples according to pairwise Dunn's rank sum post-hoc test (see Methods section for details). Note the outliers in the feces sample and in the eggs-skin comparison. C. Bar plot representation of source proportions in egg microbiomes. D. Principal coordinate analysis of microbial communities across eggs, feces and skin samples. Community composition was analyzed using PhilR distance. Percentages of explained variations are indicated on both axes.

Figure 7: Bacterial taxonomic profiles from X. tropicalis prometamorphic tadpole gut.
A. Histogram representation of bacterial diversity at the phylum level observed in a pool of five prometamorphic tadpole's guts at stage NF56. metaDNA: metagenomic analysis; metaRNA: metatranscriptomic analysis. Each color in the histogram refers to a phylum as described in the legend. B. Vizualisation of the metagenomic assembly. Each bin identified using DASTool is represented in a different colour, each circle is a contig. The circles diameter is proportional to contig length.

Figure 8: Overview of X. tropicalis tadpole's microbiota metabolic functions.
A. This barplot represents the read coverage (x-axis, in transcripts per kilobase million) on genes encoding enzymes participating in various Metacyc pathways (y-axis). B. Counts of metagenome bins, genes and scaffolds in which enzymes involved in selected biosynthetic pathways. Expressed genes encoding enzymes involved in selected KEGG modules mentioned on the y-axis were counted.